Journal of Materials Research and Technology 28 (2024) 3805–3824

Contents lists available at ScienceDirect

Journal of Materials Research and Technology

journal homepage: www.elsevier.com/locate/jmrt

Effect of NiO, ZrO_2 and TiO_2 on the formation of glass-ceramic cordierite in the $MgO–Al_2O_3–SiO_2–MoO_3$ system

Manuela Alejandra Zalapa-Garibay [a,**], Simón Yobanny Reyes-López [b,*]

[a] Instituto de Ingeniería y Tecnología, Universidad Autónoma de Ciudad Juárez, Av. Del Charro No. 450 Nte. Col. Partido Romero C.P. 32310, Chihuahua, Ciudad Juárez, Mexico

[b] Instituto de Ciencias Biomédicas, Universidad Autónoma de Ciudad Juárez, Envolvente Del PRONAF y Estocolmo S/n, C.P. 32310, Chihuahua, Ciudad Juárez, Mexico

ARTICLE INFO

Handling editor. Prof. M Meyers

Keywords:
Glass-ceramic
Cordierite
Aluminosilicates
Glassy phase
Parent glass
Magnesium molybdate

ABSTRACT

In glass-ceramic design, the two most crucial factors are composition and microstructure both factors control the ability to form a glass and determines its degree of workability. The composition also determines whether internal or surface nucleation can be achieved. If internal nucleation is desired, as is the case in hot forming glassware, right nucleating agents are melted into the glass as part of the bulk composition. For this reason, this research work focuses on obtaining glass-ceramic cordierite starting from a parent glass of the $MgO–Al_2O_3–SiO_2–MoO_3$ system, using NiO, ZrO_2 and TiO_2 in a range of 1%Wt to 3%Wt, with the objective of identifying which of the oxides most favors the formation of cordierite. Twelve samples were prepared, which were characterized by thermal gravimetric analysis (TGA), differential thermal scanning analysis (DSC), X-ray diffraction (XRD), Elemental X-ray mapping (SEM), and Infrared spectra using the ATR technique (FT-IR). It was found that NiO is the oxide that most promotes the formation of the cordierite phases, in addition to the use of molybdenum as part of the parent glass, which lowers the crystallization temperature of the crystalline phases obtained. This is determined with the results of phase quantification using the Rietveld method, by XRD, where the samples with NiO add up to a content greater than 90 % of cordierite α and β. And it is supported by the SEM results, where the characteristic hexagonal morphologies of cordierite are identified, the IR characterization results where the bands of the bonds of the phases identified by XRD are identified.

1. Introduction

Glass-ceramics are approximately 65 years old, noted for their unusual combination of properties leading to a variety of high-tech products for consumers and specialty markets. The first original definition considered was that of *Stookey* of 1958: "Glass-ceramics are manufactured by first melting and forming special glasses, which contain nucleating agents that cause controlled crystallization of the glass" [1–4]. However, due to the developments in the last six decades, *Deubener* et al. propose an updated and more complete definition: "glass-ceramics are inorganic and non-metallic materials prepared by controlled crystallization of glasses through different processing methods. They contain at least a type of functional crystalline phase and a residual glass. The crystallized volume fraction can vary from ppm to almost 100 % [2].

Describing the manufacturing process by which glass-ceramic materials are obtained, it can be said: these materials are obtained by controlled crystallization of non-metallic inorganic glasses, their microstructures comprise at least one type of functional crystal and a glassy fraction, and the volume fractions of crystals and glass above the ppm level are suitable in the definition of glass-ceramics. However, if the glasses are mixed with other crystalline materials (ceramics, metals, semiconductors, or polymers), they are composites and are not considered glass-ceramics. The same rule applies to non-glass (without Tg) amorphous precursors, and to glasses in which only metal particles precipitate after crystallization, as they are not "stabilized". Furthermore, "nucleated" glasses containing only crystalline nucleating agents are not considered glass-ceramics, since a desired functionality is typically not achieved by this desired crystallization [[2,5–7]].

One of the most used systems for manufacturing ceramic materials is the $MgO–Al_2O_3–SiO_2$ (MAS) system, due to the sizable number of experimental studies conducted over several decades. However, the

* Corresponding author.
** Corresponding author.
E-mail addresses: manuela.zalapa@uacj.mx (M.A. Zalapa-Garibay), simon.reyes@uacj.mx (S.Y. Reyes-López).

https://doi.org/10.1016/j.jmrt.2023.12.176
Received 4 July 2023; Received in revised form 15 December 2023; Accepted 19 December 2023
Available online 27 December 2023

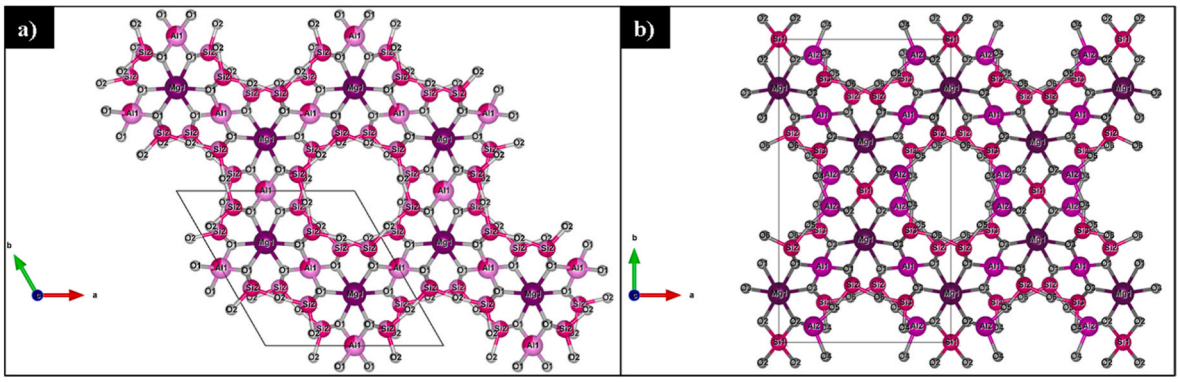

Fig. 1. a) Crystal structure of high temperature indialite or α-cordierite with hexagonal system; and b) β-cordierite with orthorhombic system), $(Si/Al)O_4$ tetrahedrons orderly arranged in $[(Si_4Al_2)O_{18}]$ hexagonal rings and among the rings, $[MgO_6]$ octahedral connected by one $[SiO_4]$ and two $[AlO_4]$ [17].

quality of these studies varies substantially, spinels have been repeatedly studied and are known in detail, equilibrium relationships for other compositions of the MAS system are only partially known and often in previous studies that have not been revisited by more modern experimental and analytical techniques [8]. Therefore, the glass-ceramic materials within this system are not the exception. Cordierite is one of the most important phases of the MAS system, due to its valuable properties and great commercial appeal. In general, cordierite has a low expansion coefficient, high resistance to thermal shock, high refractoriness, chemical stability, low thermal conductivity and dielectric constant, and good mechanical properties [9–11]. In view of the properties that it exhibits individually and as a composite material, cordierite is used in the manufacture of refractories, insulators, filters, catalytic supports, pigments, enamels, corrosion-resistant materials, among others [11,12]. Cordierite presents as the most accepted global formula $2MgO{\cdot}2Al_2O_3{\cdot}5SiO_2$, with a composition of 13.8 % MgO, 34.8 % Al_2O_3 and 51.4 % SiO_2 [9,13,14]. Natural cordierite is not pure in magnesium; it presents cations of Mg^{2+}, Al^{3+}, Si^{4+} substituted or inserted in the structure [10–17]. Natural cordierite minerals are very rare in nature and have high percentages of iron, which is why they are not used for the manufacture of ceramics [13,14]. Cordierite exhibits three forms of polymorphism (α, β and μ – cordierite) [10,14,17]; the hexagonal phase or α-cordierite is stable between 1450 °C and 1460 °C, this polymorph is also called high temperature cordierite or indialite (Fig. 1a). Orthorhombic cordierite or β-cordierite is stable below 1450 °C, it is also called low-temperature cordierite (Fig. 1b). The metastable form or μ – cordierite is a difficult phase to obtain and requires many hours for its crystallization, which occurs between 800 and 900 °C [9]. Transition metal oxides are widely used to obtain glass-ceramics because they can play two important roles in the crystallization of the phases of interest, i) They can dramatically affect the rate of nucleation, acting as nucleating agents, or ii) They can give specific properties to the glass-ceramic, acting as "active" agents [18–22].

In previous studies, transition metal ions have been used as dopants in obtaining cordierite; obtained through the crystallization of magnesium aluminosilicate glasses and cordierite glasses doped with Mg and NiO. *Golubkov* et al. [23,24] investigated the effect of the addition of NiO on the phase separation and crystallization of magnesium aluminosilicate glasses with equimolar contents of MgO and Al_2O_3 nucleated by TiO_2 and doped with 0.5–5 mol% of NiO. They observed the reduction in the crystallization capacity of the magnesium aluminosilicate phase with an increase in the NiO content leading to its complete suppression in the presence of 5 mol% NiO.

Alekseeva et al. [25] studied the phase transformations in NiO-doped magnesium aluminosilicate glasses nucleated by ZrO_2 and reported the change in absorption spectra of the material due to the entry of Ni^{2+} ions into the aluminosilicate crystal phases. *Boberski and Giess* [26] studied the isothermal crystallization behavior of stoichiometric powdered cordierite glasses containing NiO and found the existence of a complete crystalline solid solution between magnesium cordierite ($Mg_2Al_4Si5O_{18}$) and nickel cordierite ($Ni_2Al_4Si_5O_{18}$). They also concluded that the formation of nickel-containing cordierite was independent of the nickel content of the glass. Other oxides used as nucleating agents are TiO_2 and ZrO_2, in the conventional methods for obtaining cordierite, however, they present a problem when used as conventional nucleating agents, since several weight % are required to achieve nucleation suitable for glass. These agents not only provide nucleation sites for the main crystalline phases, but also precipitate to form secondary phases in the final material [27].

On the other hand, *Abdelwahab* et al. carried out a study where they varied the TiO_2/GO ratio in the SiO_2–Al_2O_3 system with the aim of observing the effect on the mechanical and electrical properties, using the sol gel method for the preparation of glass-ceramic samples. They observed that some properties such as density and friction coefficient decrease as the GO content increases, other properties such as microhardness and electrical properties showed an increase when the TiO_2/GO weight ratio was equal to 20/5 %wt [28].

Regarding research focused on the effect of MoO_3 on cordierite crystallization, *Maeda* et al. carried out a study in which small percentages of MoO_3 and WO_3 were used in the fusion of glasses from the MAS system, they determined that molybdenum oxide exerted a stronger effect on nucleation than tungsten oxide, it helped the formation of more crystals, achieving a glass-ceramic with a fine microstructure under heat treatment up to 1050 °C. Furthermore, this pair of oxides are effective as dopants at much lower concentrations than standard oxides that have been used as nucleators such as TiO_2 or ZrO_2. Therefore, MoO_3 and WO_3 could potentially improve the performance of the glass-ceramic. Molybdenum is specifically promising because it achieves glass-ceramics with a fine microstructure [29]. Finally, *Dordević* et al. added 20%wt of MoO_3 to a mixture of 80%Wt of MAS to subsequently analyze the microstructural evolution in a temperature range of 850 °C–1300 °C, with which they determined that Al_2O_3 forms intermediate compounds with MoO_3 in a range of temperature of 850 °C and 1100 °C, $MgMoO_4$ is detected after sintering MgO and MoO_3 at 850 °C and 1100 °C, they also observed the formation of the cordierite phase at 1200 °C, so they conclude that MoO_3 can be used to lower the sintering temperature and cordierite formation by more than 150 °C [30].

Although interesting studies have been conducted to examine the influence of transition element oxides such as NiO, WO_3, ZrO_2, TiO_2 and MoO_3 on the microstructural evolution of the most important phases of the MAS system and cordierite glasses, until to date, no studies have been reported with the influence of MoO_3 and the different most used dopants. Therefore, more complete data is required so that a clearer understanding of crystallization processes can emerge. In this sense, the objective of this work is to contribute to knowledge by studying the influence of NiO, TiO_2 and ZrO_2 as dopant elements in obtaining

Table 1
Atomic properties of the elements present in the samples [8].

Element	Atomic radius	Electronegativity	Valence	Atomic weight	Glass forming elements
Si	1.1	1.9	4	28.06	Network former
Al	1.25	1.61	3	26.98	Network former and Intermediate
Mg	1.5	1.31	2	24.30	Network modifier
Mo	1.45	2.16	2,3,4,5,6	95.94	Network modifier
Ni	1.35	1.91	0,2,3	58.6934	Network former
Zr	1.55	1.33	4	91.224	Network former and Intermediate
Ti	1.4	1.54	−1, 1,2,3,4	47.867	Intermediate

Table 2
Chemical composition of samples in %wt.

Sample	SiO_2 (% wt.)	Al_2O_3 (%wt.)	MgO (%wt.)	MoO_3 (%wt.)	NiO (% wt.)	ZrO_2 (% wt.)	TiO_2 (% wt.)
M7	45	22.5	10.0	22.5			
Parent Glass	52.1	26.35	11	10.55	–		
1A	51.58	26.08	10.9	10.44	1		
1B	51.06	25.80	10.8	10.34	2		
1C	50.54	25.56	10.67	10.23	3		
2A	51.58	26.08	10.9	10.44		1	
2B	51.06	25.80	10.8	10.34		2	
2C	50.54	25.56	10.67	10.23		3	
3A	51.58	26.08	10.9	10.44			1
3B	51.06	25.80	10.8	10.34			2
3C	50.54	25.56	10.67	10.23			3

cordierite, on the $MgO–Al_2O_3–SiO_2–MoO_3$ system, with the aim of obtaining a lower crystallization temperature and observing the effects of the oxides proposed as dopants, to determine which of the three has the most favorable effect on cordierite formation, which will allow modifying the mechanical properties of glass-ceramics. For this purpose, twelve samples with specific variations of 1%wt, 2%wt, and 3%wt of NiO, TiO_2 and ZrO_2 from 0 to 3 wt% were analyzed by differential thermal analysis (DTA), X-ray diffraction (XRD), scanning electron microscopy (SEM) and Infrared spectra using the ATR technique (FT-IR).

2. Materials and methods

For the preparation of the parent glass, a composition close to the stoichiometric chemical composition of cordierite was selected in the phase diagram of the MAS system [**31**]. Reagent grade powders of MgO (99 %, 325 mesh), Al_2O_3 (99 %, 325 mesh), SiO_2 (99 %, 325 mesh), MoO_3 (99 %, 325 mesh), NiO (nanoparticles, <150 nm, 95 %) TiO_2 (nanoparticles, <150 nm, 95 %) and ZrO_2 (nanoparticles, <150 nm, 95 %) were used, which were bought from the Sigma Aldrich® Company. Table 1 shows the atomic properties of the elements present in the parent glass and the role they play in the formation of glass. For the preparation of the parent glass, the chemical composition of the mixture called M7 was used (See Table 2). Once the mixture was weighted, it was subject to a mixing process for 2 h at 350 rpm, in a RESTCH model PM 400 planetary mill. Once the mixture was obtained, it was melted in a platinum crucible using the same oven, with a ramp of heating at 7 °C/s, until reaching the maintenance temperature of 1600 °C and kept there for 2 h. Subsequently, it was subject to cooling by thermal shock, using water at room temperature, thus obtaining the glassy phase. After obtaining the parent glass, it was subject to XRD to determine its amorphous phase, it was also characterized by Inductively Coupled Plasma Mass Spectrometry (ICP-MS) to determine its chemical composition (See Table 2). The parent glass was subject to a grinding process, using the RESTCH PM 400 brand mill, at a speed of 350 rpm for 5 h, and a zirconium container, resulting in fine powders of parent glass with a particle size within the 1.02–3.45 μm range (determined by scanning electron microscope; FESEM SU5000 Hitachi). Subsequently, the mixtures for the preparation of the samples were made by adding oxides (NiO, TiO_2 and ZrO_2) as nucleants in quantities of 1%wt, 2%wt and 3% wt to the parent glass. The samples were identified as 1A, 1B, 1C, 2A, 2B, 2C, 3A, 3B and 3C, as shown in Table 2. To prepare the solid samples, an MTI brand uniaxial hydraulic press was first used with a pressure of 2 Ton for 1 min, giving samples of 0.5 inches in diameter. To find the sintering temperature of the samples, the parent glass was characterized using the differential scanning calorimetry (DSC) technique, with which it was determined that the phase of interest (cordierite) can be obtained at 1200 °C, once the sintering temperature was determined, the rest of the samples (1A, 1B, 1C, 2A, 2B, 2C, 3A, 3B and 3C) were prepared and subjected to heat treatment using a Thermo Scientific HERATHERM drying oven. The drying treatment was conducted at a temperature of 100 °C for a period of 2 h, to eliminate traces of moisture before subjecting them to the sintering process. The sintering of the samples was conducted at a temperature of 1200 °C and a dwelling time of 2 h, in the same oven that the fusion of the parent glass was carried out. For structural and compositional characterization, the samples were milled

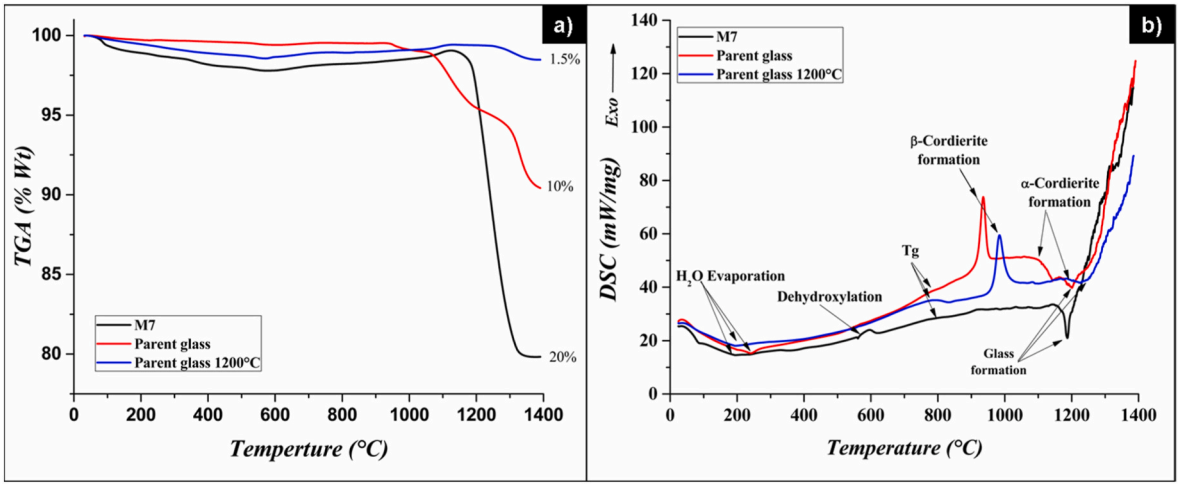

Fig. 2. a) TGA and b) DSC of samples M7, Parent glass and parent glass sintered at 1200 °C.

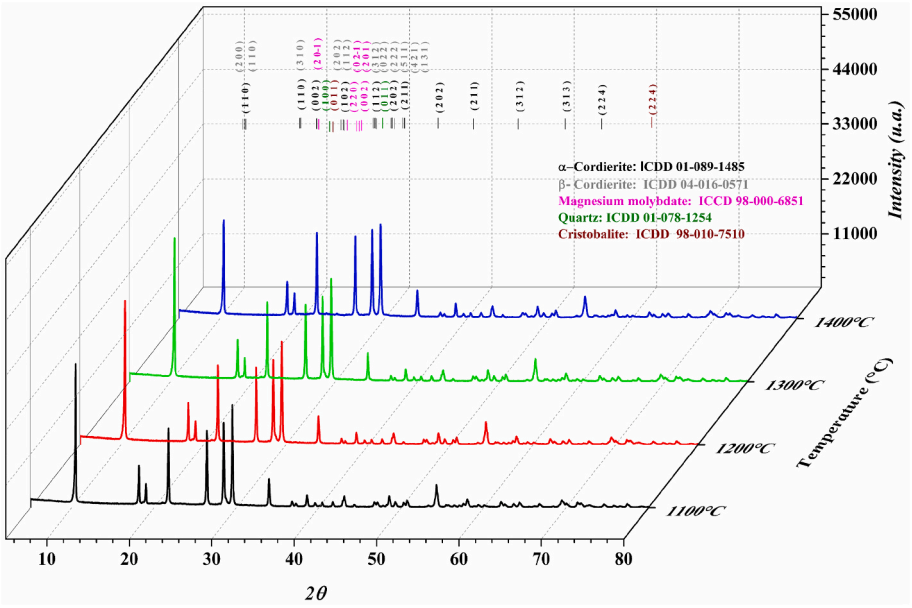

Fig. 3. X-ray diffraction of sintered parent glass in a temperature range of 1100 °C–1400 °C.

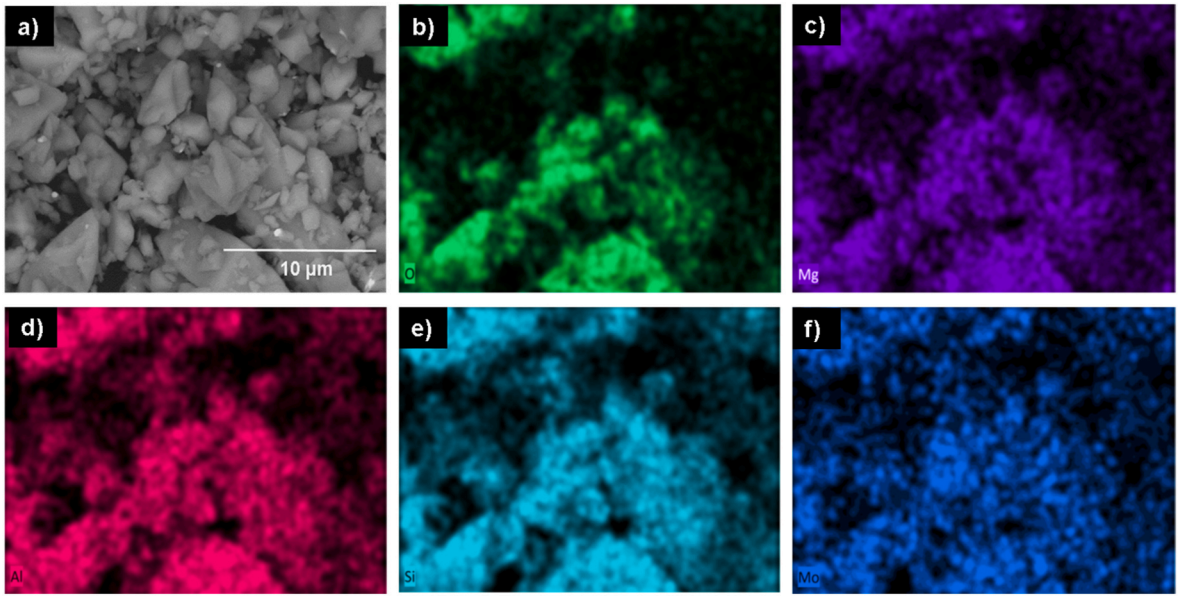

Fig. 4. X-ray mapping of the parent glass, a) backscattered electrons, b) Oxygen, c) Magnesium, d) Aluminum, e) Silicon, and f) Molybdenum

in the RESTCH 400 mill for 30 min at 250 rpm.

The compositional and structural study of each of the samples obtained was conducted using the following techniques, TGA and DSC using a TA Instruments Q600 brand equipment, with which the sequence of thermal decomposition in an air atmosphere was determined, in a temperature range of 100 °C to 1400 °C, using a heating ramp of 10 °C/min. The evolution of the crystalline phases as a function of temperature was determined by X-ray diffraction using a Panalytical Empyrean X-ray diffractometer with a Cu X-ray source (Kα = 1.5405 Å), and for the identification of the phases the database of the International Centre for Diffraction Data (ICDD) was used. For the characterization by scanning electron microscopy (SEM), a FESEM SU5000 Hitachi microscope was used. Finally, for the characterization by infrared spectrometry, an Alpha Platinum FT-IR (Bruker Optics Inc) series equipment was used to obtain infrared spectra using the ATR technique with diamond crystal, the spectra were accumulated in 64 scans at 2 cm^{-1}.

2.1. Results

Once the samples were prepared with the compositions specified in Table 1, and after applying the heat sintering treatment at 1200 °C with a dwelling time of 2 h, the characterization continued in the order mentioned below.

2.1.1. Parent glass

A thermal analysis was carried out to examine the development of the phases in the M7 sample, the parent glass, with the aim of determining the optimum sintering temperature of the samples to which oxides were added as nucleating agents. This analysis was carried out in a temperature range of 25–1400 °C. It can be seen in Fig. 2a that the three samples show a weight loss of less than 2 % in a temperature range of 25–550 °C, which can be attributed to water loss. Sample M7 remains constant from 550 to 1150 °C, however at 1150 °C a significant weight

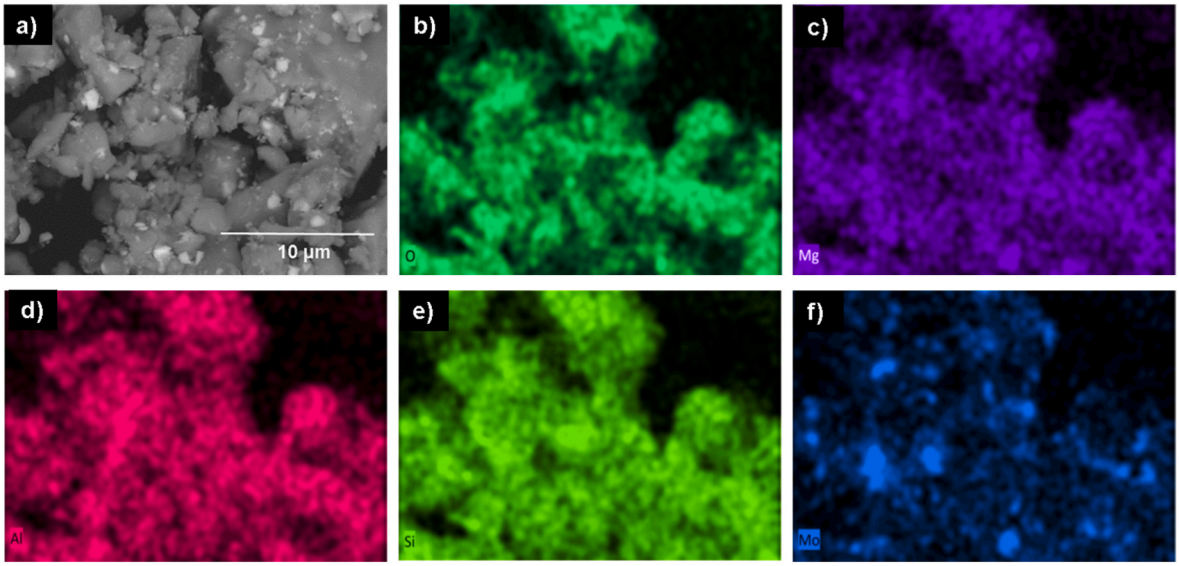

Fig. 5. Elemental X-ray mapping of the parent glass sintered at 1200 °C, a) backscattered electrons, b) Oxygen, c) Magnesium, d) Aluminum, e) Silicon, and f) Molybdenum.

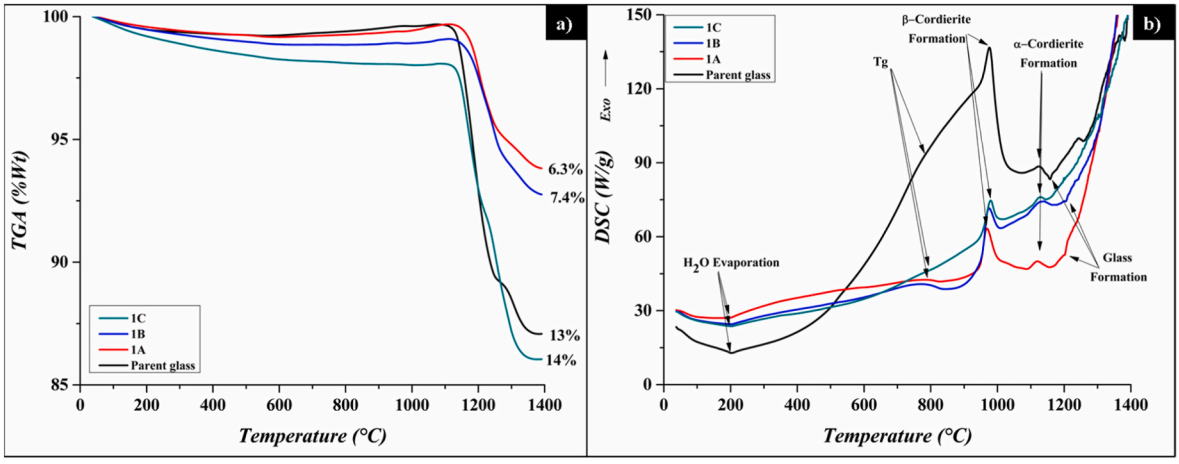

Fig. 6. a) TGA and b) DSC of Parent glass, samples 1A, 1B and 1C sintered at 1200 °C.

loss of 18 % begins, which can be related to the evaporation of MoO_3 [31]. In the case of the parent glass sample, the sample weight remains constant up to 950 °C, followed by a 0.5 % weight loss over a temperature range of 950–1000 °C which can be associated to the loss of MoO_3. Subsequently there is a weight loss of 3 % from 1000 to 1180 °C also associated with the loss of MoO_3, conclusively a weight loss of 6 % is observed in a temperature range of 1180 at 1400 °C attributed to the formation of glass in addition to the loss of MoO_3, finally in the sintered parent glass sample a total weight loss of 1.5 % is observed associated with the evaporation of MoO_3 during melting glass [31–34].

The DSC results are shown in Fig. 2b, were an endothermic peak around 200 °C can be observed for all cases and it is related to the effect of loss of residual water in the sample. In the case of the sample M7, an exothermic peak is observed at 600 °C related to dehydroxylation, then the glass transition temperature (Tg) is observed for the three cases, in a temperature range of 790–820 °C, where it is highlighted that it is easier to identify the Tg for the parent glass sample sintered at 1200 °C, because it is a crystalline sample [32]. Continuing with the analysis of the curves we can observe that for the parent glass sample and parent glass sintered at 1200 °C there is a pronounced exothermic peak at temperatures of 930 and 990 °C respectively, which are attributed to the formation of cordierite β, and because it is a less stable phase than the α phase, a higher energy is needed for its crystallization, as can be seen in the small exothermic peak that occurs at a temperature of 1200 °C for the parent glass sample, which corresponds to the crystallization of the α cordierite. There is an endothermic peak in the three samples that can be attributed to the beginning of melting glass, in the M7 sample it is located at 1190 °C, in the parent glass sample it is located at 1200 °C and in the parent glass sample sintered is placed at 1220 °C [30,32,33]. With the analysis of the DSC curves, and considering that the thermal analyses were conducted at a speed of 10 °C/min, the curve of the sample M7 does not present a crystallization of phases because we are starting from a mixture of oxides and before crystallization the formation of glass begins, in the case of the parent glass sample, it crystallizes to some degree but not completely due to the speed at which the analysis was carried out, and finally in the parent glass sample sintered at 1200 °C, it is observed that the energy necessary for the crystallization of the retained glass is lower with respect to the other two samples, due to the fact that it is a glass-ceramic sample. Considering the results of the TGA and DSC analyses, it can be determined that the stepped weight loss observed in the parent glass sample can be directly attributed to MoO_3 evaporation, however the partial MoO_3 retention is attributed to the

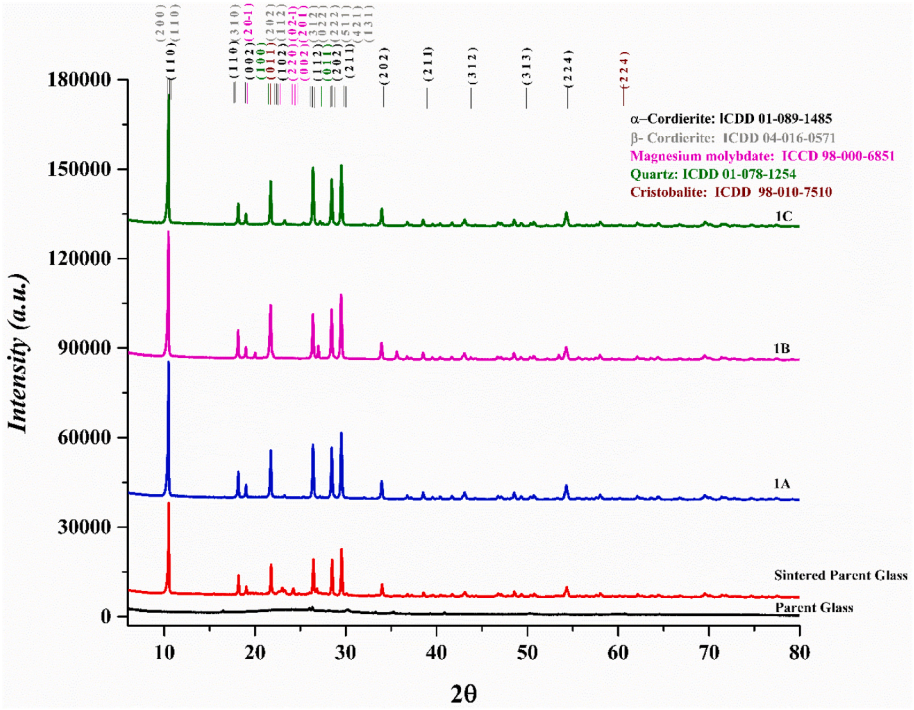

Fig. 7. X-ray diffraction of sample of parent glass, Sintered parent glass at 1200 °C, 1A, 1B y 1C.

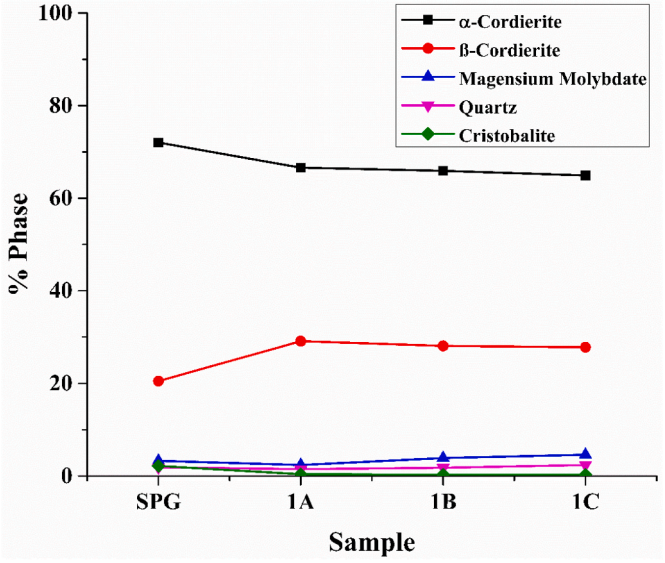

Fig. 8. X-Ray Diffraction Rietveld analysis at 1200 °C for samples parent glass, sintered parent glass (SPG), 1A, 1B y 1C.

crystallization of the main phases and the formation of glass; because Molybdenum is likely to become part of the crystalline structure of the phases that are formed in the temperature range of 1000 °C–1400 °C, as mentioned by *Đorđević* et al. [30,31].

In Fig. 3, the diffractograms of the sintered glass sample are shown, were the result of the thermal analyses were taken as a reference and 4 samples were sintered in a temperature range of 1100–1400 °C. It is observed that the main phases that occur in the temperature range of 1100–1400 °C are α-cordierite, β-cordierite, magnesium molybdate, quartz and cristobalite. The diffractograms of the sintered samples at 1100, 1200 and 1300 °C keep the same intensities in the reflections, which shows that the crystallinity is similar, however the percentages of each phase in each sample may vary slightly. On the other hand, a decrease in the intensities of the reflections is observed in the sample sintered at 1400 °C, which is attributed to the dissolution of crystals as observed in the DSC curve. Therefore, the temperature of 1200 °C is chosen to sinter the samples with nucleating oxides.

In Fig. 4, the results of elemental X-ray mapping of the parent glass are shown, where it is observed that the composition of the sample is almost homogeneous, only a few small clear spots can be observed, which may be small concentrations of Molybdenum, the rest of the observed area is homogeneous because it is in a glassy state without forming any specific crystalline phase. Fig. 5 shows the results of the X-ray mappings of the parent glass sample sintered at 1200 °C, in this case it is observed that the morphology of the particles differs in size with respect to the parent glass sample, due to the fact that only the vitreous phase is present in the parent glass sample; also in Fig. 5, there are small concentrations of elements, which is attributed to the formation of specific phases within a vitreous matrix, such as cordierite, Magnesium molybdate, quartz and cristobalite, as determined by means of the X-Ray Diffraction technique.

2.1.2. *Parent glass + NiO*

Fig. 6a shows the TGA carried out on the parent glass, 1A, 1B and 1C samples, since with this technique it is not possible to structurally identify any material, the technique is defined solely to identify weight losses. It is observed that the parent glass sample and 1C show a weight loss of 13 % and 14 % respectively, the weight losses for samples 1A and 1B show a weight loss of 7 % and 8 % respectively, the weight losses are associated with the evaporation of the MoO_3 that is still present in the parent glass. Some aspects that we can highlight from the TGA is that when 3 % NiO is added, the behavior is similar to that of the parent glass, with this it can be determined that there may be an agglomeration of Molybdenum, therefore it is not integrated into the crystalline phases that are being formed, otherwise with sample 1A and 1B, in this case it is likely that Molybdenum is retained because it forms part of the crystalline phases that are forming. The DSC for the parent glass sample, 1A, 1B and 1C, can be seen in Fig. 6b, the endothermic peak that occurs at 200 °C corresponds to the evaporation of residual moisture retained by

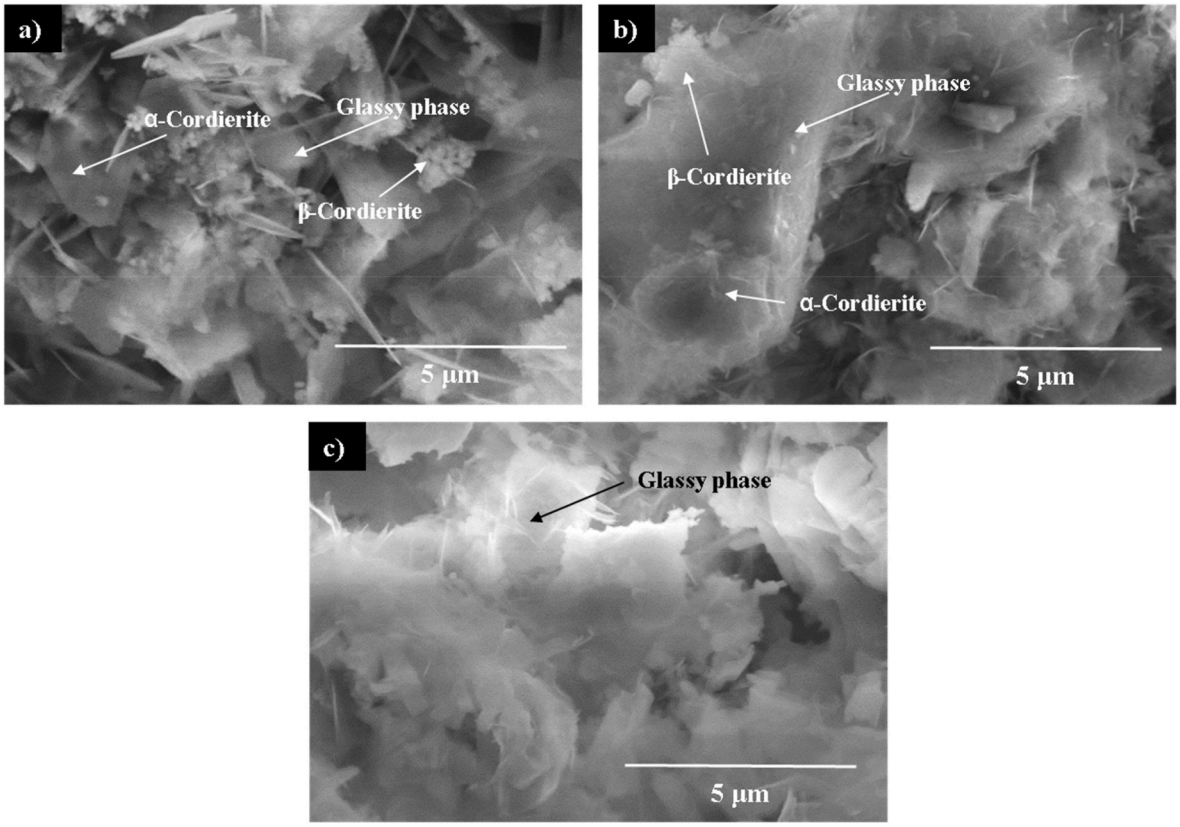

Fig. 9. Samples sintered at 1200 °C for 2 h, SEM secondary electrons, a) 1A, b) 1B and c) 1C.

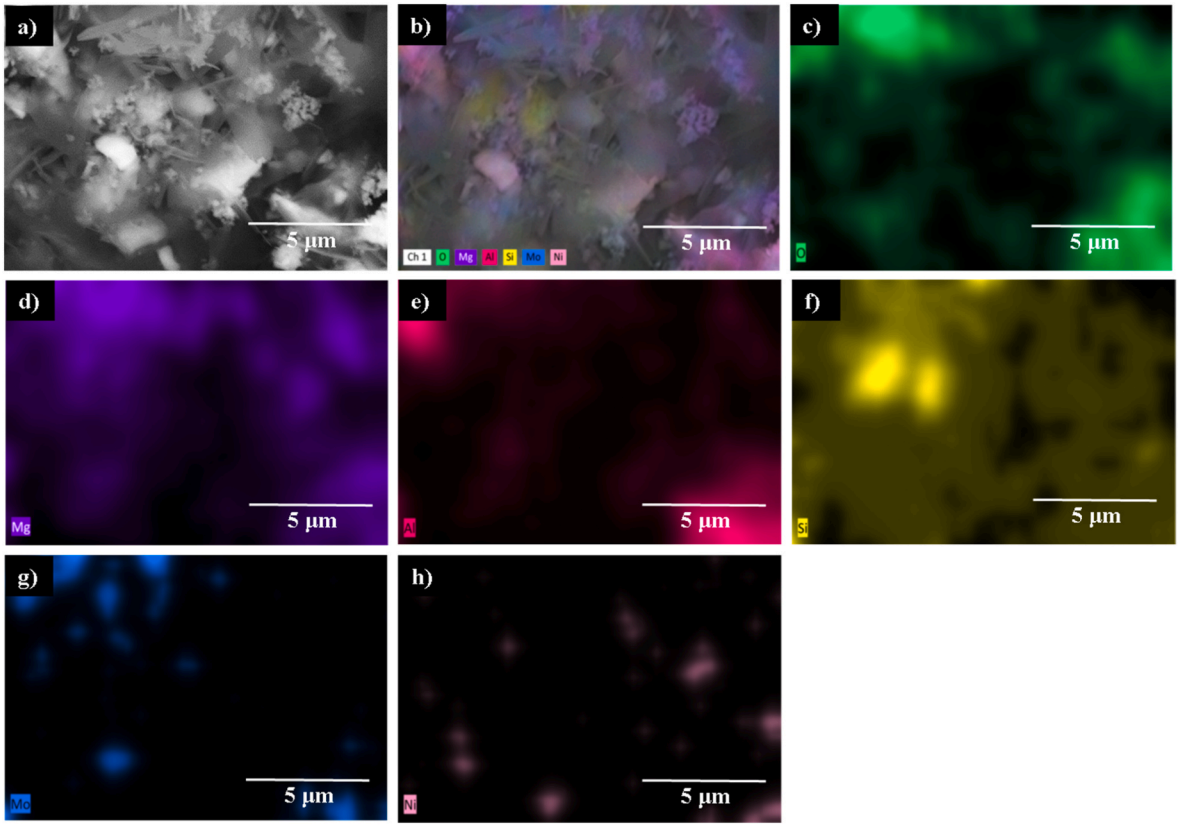

Fig. 10. Sample 1A sintered at 1200 °C for 2 h, a) backscattered electrons, b) Mapping of the constituent elements, c) Oxygen, d) Magnesium, e) aluminum, f) Silicon, g) Molybdenum and h) Nickel.

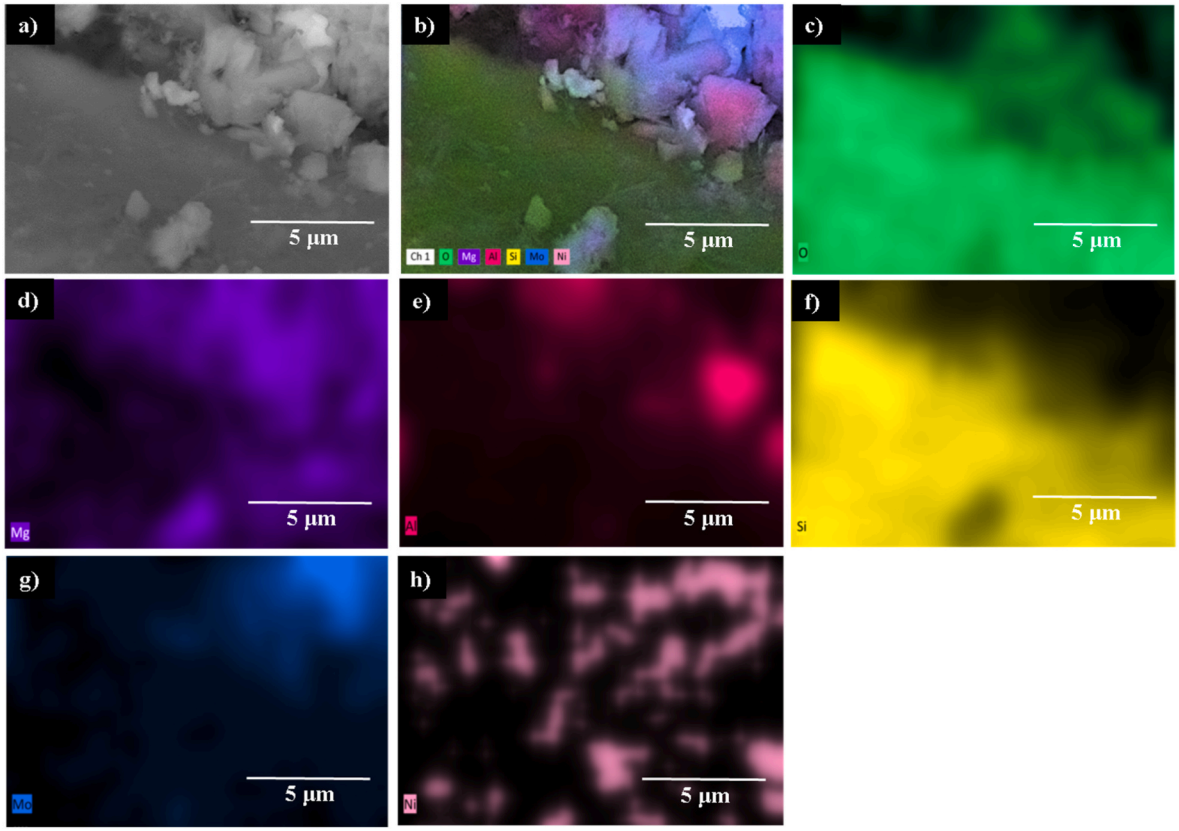

Fig. 11. Sample 1B sintered at 1200 °C for 2 h, a) backscattered electrons, b) Mapping of the constituent elements, c) Oxygen, d) Magnesium, e) aluminum, f) Silicont, g) Molybdenum and h) Nickel. In the case of the FT-IR spectrum of the Sintered Parent Glass, two bands are observed that can be attributed to the glassy phase at 450 cm^{-1} 910 cm^{-1}, the band at 450 cm^{-1} corresponds to the bending vibration of Si–O–Si in [SiO_4]-tetrahedron. The band that is close to 910 cm^{-1} and can be related to the symmetrical stretching vibration of the Si–O–Si bond [35,36]. The band observed at 764 cm^{-1} corresponds to the stretching vibration of the Mo–O bond that is associated with the magnesium molybdate phase that was identified by XRD [37]. The 482 cm^{-1}, 605 cm^{-1} and 1084 cm^{-1} bands correspond to the quartz and cristobalite phases that were identified by XRD; the band at 482 cm^{-1} can be attributed to bending vibration of Si–O bond, and the bands at 605 cm^{-1} and 1084 cm^{-1} are attributed to the asymmetric stretching vibration of the Si–O bond [36,38,39].

the sample, in a range from 791 to 806 °C the glass transition temperature is presented for the four samples where it is observed that in the case of sample 1B it is revealed more clearly, because the phases crystallize more easily compared to the three other samples, in the range of 967–979 °C an exothermic peak is presented and corresponds mainly to the crystallization of the cordierite phase. Following the DSC curve a small exothermic peak is observed at 1120 °C for the three samples corresponding to the crystallization of α cordierite and secondary phases such as SiO_2, silicates and aluminosilicates [32,33]. Finally, an endothermic peak is observed in a range between 1160 °C and 1180 °C, which corresponds to the melting of the crystals.

Fig. 7 shows the diffractograms of the parent glass sample, parent glass sintered at 1200 °C, 1A, 1B and 1C, with the aim of observing the difference in the intensities of the reflections of the main phases when adding the NiO as nucleant, firstly it is observed that the parent glass sample is amorphous, then the sintered parent glass sample is observed at 1200 °C where the phases of cordierite α, cordierite β, magnesium molybdate, quartz and cristobalite are identified. Adding NiO increases the intensities of the reflections of the main phases, therefore NiO promotes the formation of the main phases such as cordierite α and cordierite β, taking as reference the previous study carried out by Boberski and Giess, Nickel could be an active part of the cordierite structure and also functions as a nucleating agent for crystal formation [26].

Fig. 8 shows the results of the phase quantification analysis by the Rietveld method with the support of the High Score plus® software. It is observed that the α-cordierite is the phase with the highest percentage in all the samples, even though when adding NiO, cordierite decreases approximately 5 %, β-cordierite increases 9 %, so when adding the two phases, more than 90 % Cordierite is obtained in all samples. It is important to mention that NiO does not form secondary phases, therefore it can be suggested that it enters the cordierite structure, and considering its electronic properties (Table 1), Ni can eventually take the positions of Al.

On the other hand, the secondary phases formed are magnesium molybdate, cristobalite and quartz, the sum of the percentage by weight of the three is approximately 7.5 % in the sample without NiO, in this case adding NiO decreases the percentage of the secondary phases because the cordierite phase increases.

Fig. 9 shows the morphologies obtained by SEM analysis in samples 1A, 1B and 1C after the heat treatment. In Fig. 9a, which corresponds to sample 1A with a content of 1 % Wt. of NiO, hexagonal platelets characteristic of the beginning of the crystallization of the glass-ceramic cordierite α are observed [**35**], the morphology of the cordierite β and some glassy-phase particles are also identified, due to the fact that the samples were crushed for analysis, the hexagons can be appreciated separated, in Fig. 9b the characteristic hexagon of the hexagonal cordierite is observed within the glassy phase, in addition to identifying the β cordierite phase, in Fig. 9c the glassy phase is observed, however they it is not readily identifiable to the naked eye as the α and β cordierite primary phases.

Figs. 10–12 show the results of the Elemental X-ray mapping for samples 1A, 1B and 1C respectively, where the presence of oxygen, magnesium, aluminum, silicon, molybdenum, and nickel is observed. In the case of sample 1A (Fig. 10) a homogeneous distribution of oxygen,

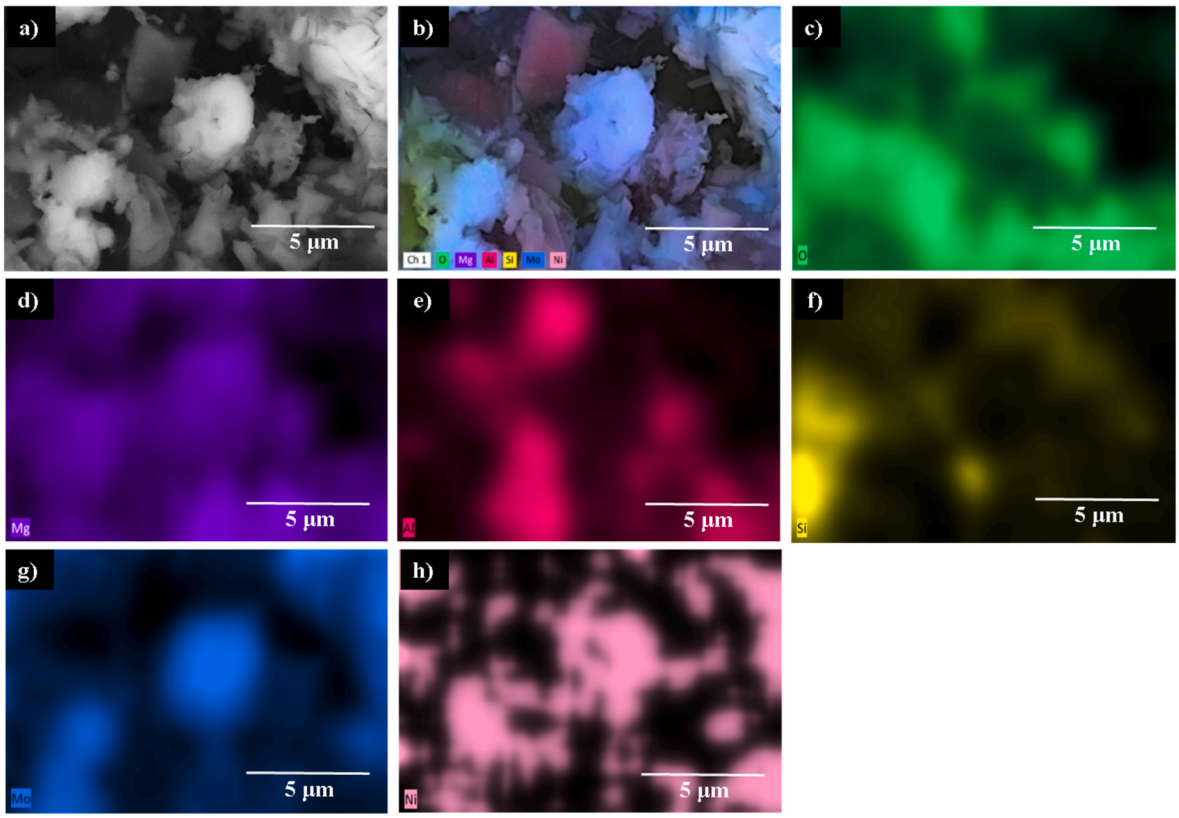

Fig. 12. Sample 1C sintered at 1200 °C for 2 h, a) backscattered electrons, b) Mapping of the constituent elements, c) Oxygen, d) Magnesium, e) aluminum, f) Silicon, g) Molybdenum and h) Nickel. The FT-IR spectra of samples 1A, 1B and 1C sintered at 1200 °C are similar, according to the XRD results they hold the same phases with a small percentage difference. In the three spectra a band is observed at 450 cm^{-1} that corresponds to the bending vibration of Si–O–Si in the [SiO4]-tetrahedron, which is characteristic of the parent glass or glassy phase. The 479 cm^{-1}, 605 cm^{-1}, 790 cm^{-1}, 1055 cm^{-1} and 1084 cm^{-1} bands correspond to the quartz and cristobalite phases. The 479 cm^{-1} band can be attributed to bending vibration of the Si–O bond. The bands at 605 cm^{-1}, 1055 cm^{-1} and 1084 cm^{-1} are attributed to the asymmetric stretching vibration of the Si–O bond, the band at 790 cm^{-1} corresponds to the symmetric stretching vibration of the Si–O bond [[39–41]]. The 752 cm^{-1} and 821 cm^{-1} band correspond to the stretching vibration of the Mo–O bond, the 890 cm^{-1} band corresponds to the stretching vibration of the Mo–*O*–Mo bond and the band at 920 cm^{-1} correspond to the stretching vibration of the Mo═O bond, these 4 bands are attributed to the magnesium molybdate phase that was identified by XRD [37]. The bands found at 561 cm^{-1}, 650 cm^{-1}, 700 cm^{-1}, 840 cm^{-1}, 955 cm^{-1} and 1166 cm^{-1}, correspond to the cordierite phase. The 561 cm^{-1} band is attributed to the characteristic vibration of the Al–O bond, the 650 cm^{-1} band corresponds to the Mg–O bond, the at 700 cm^{-1} and 840 cm^{-1} could be attributed to symmetrical stretching vibration of the Al–*O*–Al bond in [AlO_4]-tetrahedron, the bands at 955 cm^{-1} and 1166 cm^{-1} are identified as vibrations of the Al–O bond inside a tetrahedron [29,36,42–46]. Finally, the bands found at 525 cm^{-1} and 685 cm^{-1} are the characteristic vibrations that correspond to the Ni–O bond [44].

magnesium and silicon; aluminum concentrations in specific areas and small concentration zones of molybdenum and nickel are also observed. In sample 1B (Fig. 11), a homogeneous distribution of oxygen and silicon in the vitreous zone, while magnesium, aluminum and molybdenum are concentrated in another specific area that corresponds to the characteristic phases such as cordierite and magnesium molybdate, and nickel is distributed throughout the image. Sample 1C (Fig. 12) shows the concentration of oxygen, magnesium, aluminum and silicon in the same area, which indicates homogeneity in the material; the vitreous phase and crystalline phases may be present within the same area; Molybdenum presents points of higher concentration, which indicates that the higher percentage of nickel helps the formation of magnesium molybdate and reduces the possibility of increasing the quantity of the phases of interest in the sample.

Fig. 13 shows the IR spectra for the parent glass sample, parent glass sintered at 1200 °C, 1A, 1B and 1C. For the FT-IR spectra of the parent glass, four main bands are identified, the band at 450 cm^{-1} corresponds to the bending vibration of Si–O–Si in [SiO_4]-tetrahedron. The band at 700 cm^{-1} is attributed to the symmetrical stretching vibration of the Al–*O*–Al bond in the [AlO_4]-tetrahedron. The band at 800 cm^{-1} corresponds to the interaction of Si–*O*–Si tetrahedral bridging bonds in SiO_2. The band is close to 910 cm^{-1} may be related to the symmetrical stretching vibration of the Si–O–Si bond. The band at 1097 cm^{-1} corresponded to the asymmetric stretching vibration of the Si–*O*–Si bond in the [SiO4]-tetrahedron [35,36].

2.1.3. *Parent glass + ZrO_2*

Fig. 14a shows the TGA performed on the parent glass samples, 2A, 2B and 2C; it is observed that the parent glass sample and 2C show a weight loss of 13 % and 14.2 % respectively, the weight losses for samples 2A and 2B show a weight loss of 6.9 % and 7.48 % respectively, ZrO_2 has a very similar effect to that of NiO in the parent glass when used as a nucleant, therefore weight losses are associated with the evaporation of the MoO_3 that is still present in the parent glass, in the case of sample 2C it is observed that when adding 3 % ZrO_2 the behavior is similar to that of the parent glass; with this it can determine that there may be an agglomeration of molybdenum, therefore it is not integrated into the crystalline phases that are being formed, otherwise with sample 2A and 2B, in this case it is likely that molybdenum is retained because it is part of the crystalline phases that are forming. The DSC for the parent glass sample, 2A, 2B and 2C, can be seen in Fig. 14b; the endothermic peak that occurs at 200 °C corresponds to the evaporation of residual water retained by the sample, later in a range from 791 to 804 °C, the glass transition temperature is presented for the four samples where it is

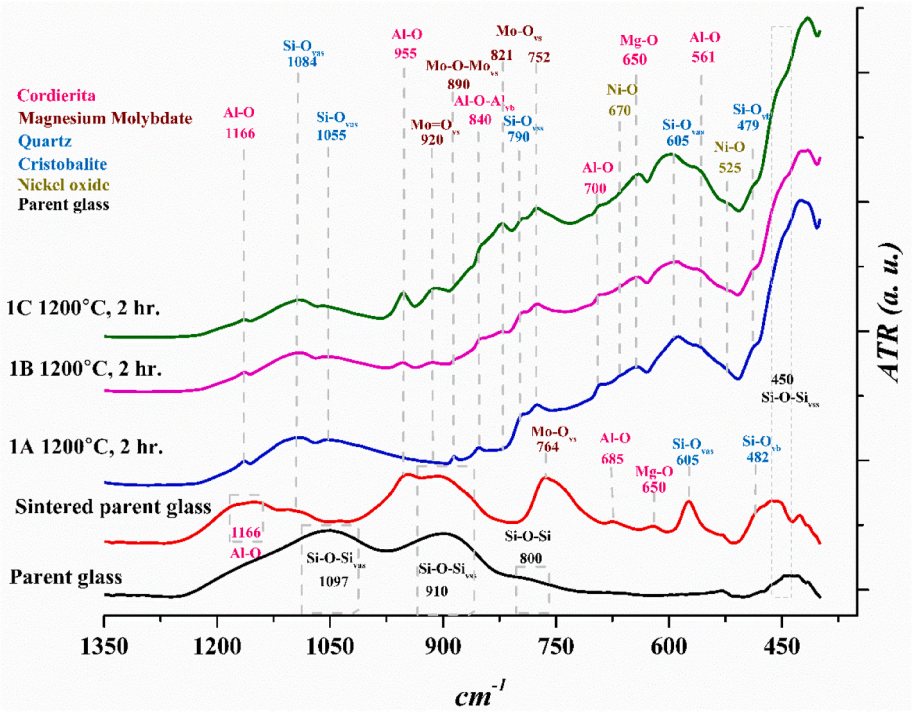

Fig. 13. Infrared spectra of samples after heat treatment at 1200 °C for samples parent glass, sintered parent glass, 1A, 1B y 1C.

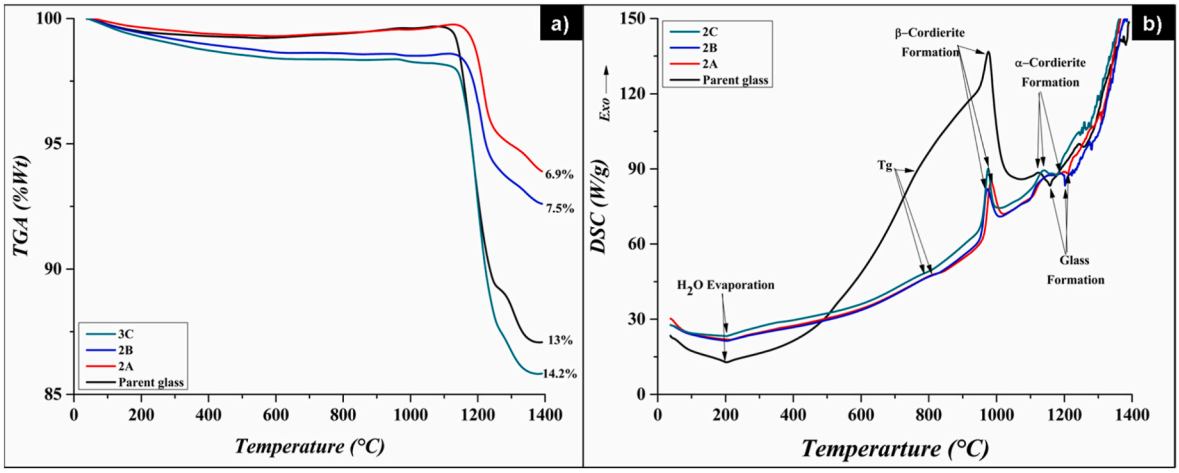

Fig. 14. a) TGA and b) DSC of Parent glass, samples 2A, 2B and 2C sintered at 1200 °C.

observed that in the case of sample 2A it is revealed more clearly, because the phases crystallize more easily compared to the others. Three other samples, in the range of 970 °C to 984 °C present an exothermic peak that corresponds mainly to the crystallization of the cordierite phase. Following the DSC curve a small exothermic peak is observed at 1120 °C that corresponds to the crystallization of α cordierite and secondary phases such as SiO_2, silicates and aluminosilicates. Finally, an endothermic peak is observed in a range from 1150 °C to 1210 °C that corresponds to the melting of the glass, the parent glass sample has the lowest glass melting temperature and the sample 2B has the highest.

Fig. 15 shows the diffractograms of the parent glass, parent glass sintered at 1200 °C, 2A, 2B and 2C samples, when using ZrO_2 as nucleant, the crystalline phases identified are the following, cordierite α, β-cordierite, mullite, magnesium molybdate, zirconium silicate, quartz and cristobalite, ZrO_2 has a similar effect on the parent glass as NiO, promoting crystallization of the main phases, this is observed in the increase of the intensity of the reflections of the phases present, unlike NiO, ZrO_2 has a greater affinity with SiO_2, for this reason it tends to form zirconium silicate as a secondary phase, which decreases the percentage of cordierite in the material.

Fig. 16 shows the results of the phase quantification by the Rietveld method with the support of the High Score plus® software. In this case, a slight decrease in the sum of the percentage of cordierite phases is seen in comparison with the samples holding NiO (Fig. 8). As in the case of the samples that hold NiO, the α-cordierite is the phase with the highest percentage in all the samples, followed by the β-cordierite, when adding values in the percentage range of 86.4 %–94.4 %, they are obtained. As the percentage of ZrO_2 increases, the sum of the total percentage of cordierite phases (α-cordierite + β-cordierite) decreases, since ZrO_2 forms zirconium silicate as a secondary phase in addition to the secondary phases that form in the case of samples holding NiO. The formation of zirconium silicate causes the decrease in the formation of cordierite, due to its affinity for SiO_2.

Fig. 17 shows the morphologies obtained by SEM analysis in samples

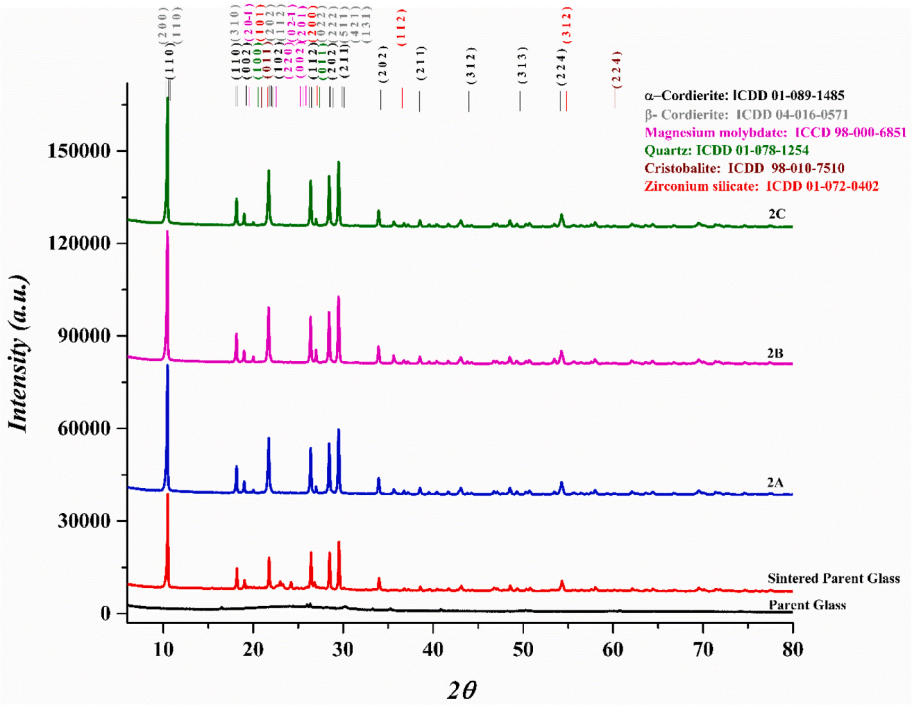

Fig. 15. X-ray diffraction of sample of parent glass, Sintered parent glass at 1200 °C, 2A, 2B y 2C.

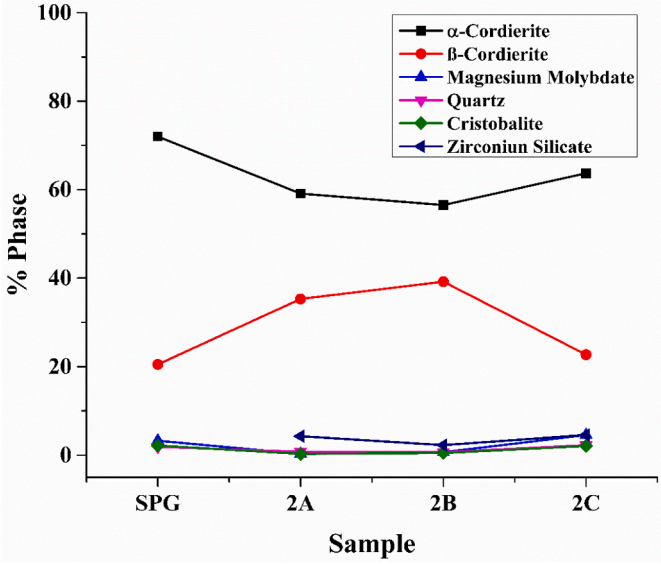

Fig. 16. X-Ray Diffraction Rietveld analysis at 1200 °C for samples parent glass, sintered parent glass, 2A, 2B y 2C.

2A, 2B and 2C after heat treatment, in Fig. 17a which corresponds to sample 2A with a content of 1%Wt of ZrO_2, hexagonal flakes characteristic of the beginning of crystallization of the glass-ceramic α-cordierite are observed, the morphology of the β-cordierite and some glassy phase particles are also identified, in this case no characteristic hexagonal morphologies of the cordierite are observed. Fig. 17b shows the morphology of β-cordierite and some glassy phase particles; Fig. 17c shows the glassy phase and some hexagonal particles corresponding to α-cordierite in addition to the morphology of β-cordierite.

Figs. 18–20 show the results of the Elemental X-ray mapping for samples 2A, 2B, and 2C, respectively, where the presence of oxygen, magnesium, aluminum, silicon, molybdenum and zirconium is observed; in the case of sample 2A (Fig. 18) a homogeneous distribution of oxygen, magnesium, aluminum, silicon and molybdenum is observed, which shows that there is homogeneity in the sample and the presence of the characteristic phases, silicon is concentrated in a small specific area corresponding to glassy-phase particles. In sample 2B (Fig. 19), a homogeneous distribution of oxygen, magnesium, aluminum, molybdenum, and zirconium is observed, which indicates that there is homogeneity in the sample and the presence of the phases of interest, there is also the presence of the vitreous phase which is identified with the concentration of silicon. In sample 2C (Fig. 20) a homogeneous distribution of oxygen, magnesium, silicon, molybdenum, and zirconium is observed, which favors the formation of the phases of interest; in this case small concentrations of aluminum are observed, which may correspond to the formation of secondary phases such as mullite.

Fig. 21 shows the FT-IR spectra for the parent glass sample, parent glass sintered at 1200 °C, sample 2A, 2B and 2C. In this case, all the bands found in the samples holding NiO appear (Fig. 13). Additionally, it is possible to identify the bands at 525 cm^{-1} and 642 cm^{-1} that correspond to the vibrations of the Zr–O bond [43,47].

2.1.4. *Parent glass + TiO_2*

Fig. 22a shows the TGA performed on the parent glass samples, 3A, 3B and 3C, where it is observed that the parent glass sample shows a weight loss of 13 %, the weight losses for samples 3A, 3B and 3C show a weight loss of 14.89 %, 14.57 % and 14.53 %, compared to the other two nucleants used (NiO and ZrO_2); in this case it is observed that the Samples have a greater weight loss and a very similar behavior between them, which can be attributed to the fact that TiO_2 in a glass-breaking oxide gets into its network and tends to form secondary phases. The DSC for the parent glass sample, 3A, 3B and 3C, can be seen in Fig. 22b, where the endothermic peak that occurs at 200 °C corresponds to the evaporation of residual water retained by the sample; in a range from 777 to 804 °C the glass transition temperature is presented for the four samples where it is observed that samples 3A, 3B and 3C follow a very similar trajectory; in the range from 977 to 985 °C there is an exothermic peak that corresponds mainly to the crystallization of α cordierite, following the DSC curve a small exothermic peak is observed at 1120 °C

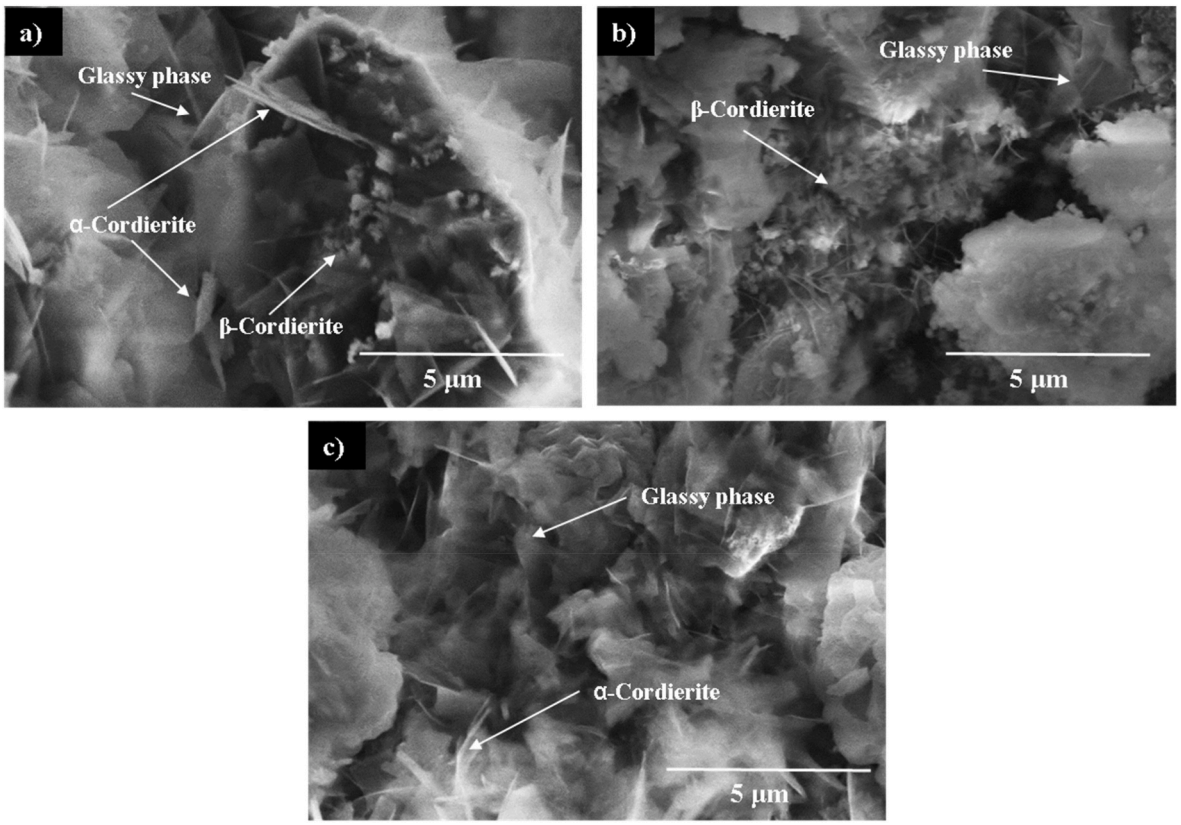

Fig. 17. Samples sintered at 1200 °C for 2 h, SEM secondary electrons, a) 2A, b) 2B and c) 2C.

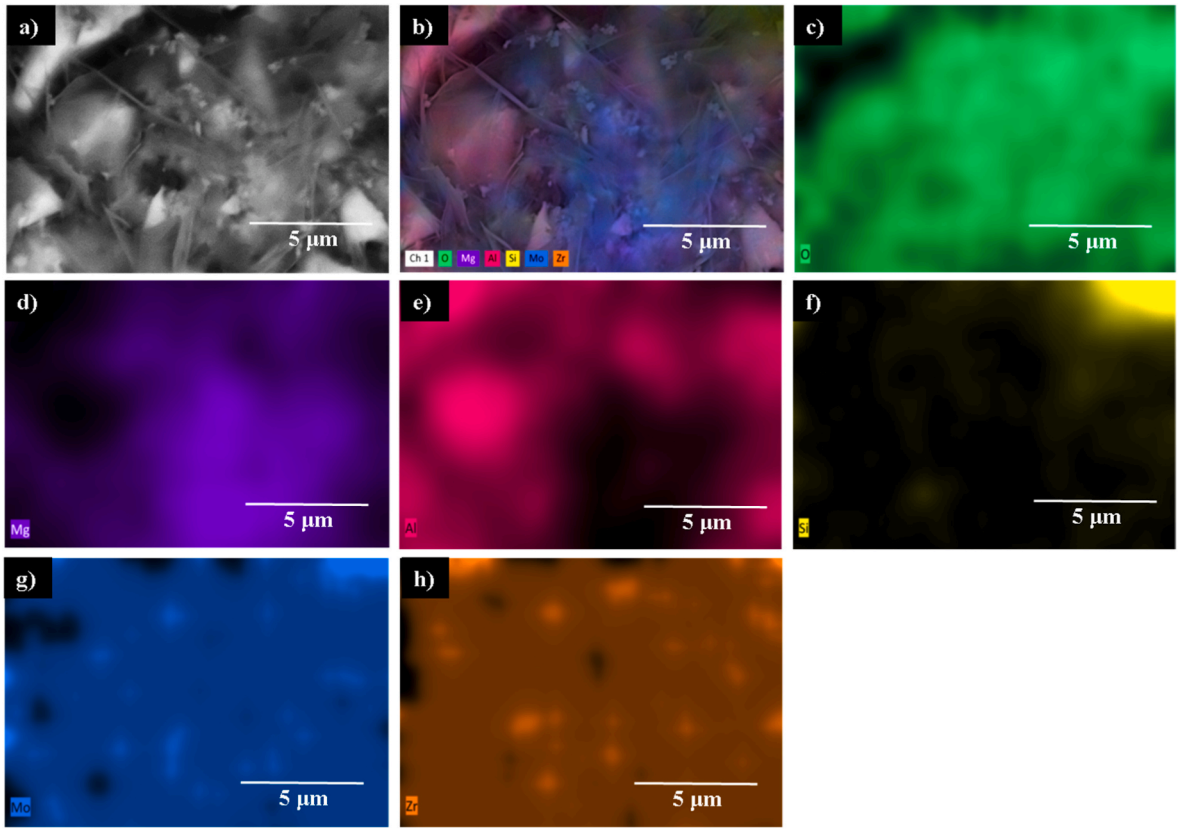

Fig. 18. Sample 2A sintered at 1200 °C for 2 h, a) backscattered electrons, b) Mapping of the constituent elements, c) Oxygen content, d) Magnesium, e) aluminum, f) Silicon, g) Molybdenum and h) zirconium.

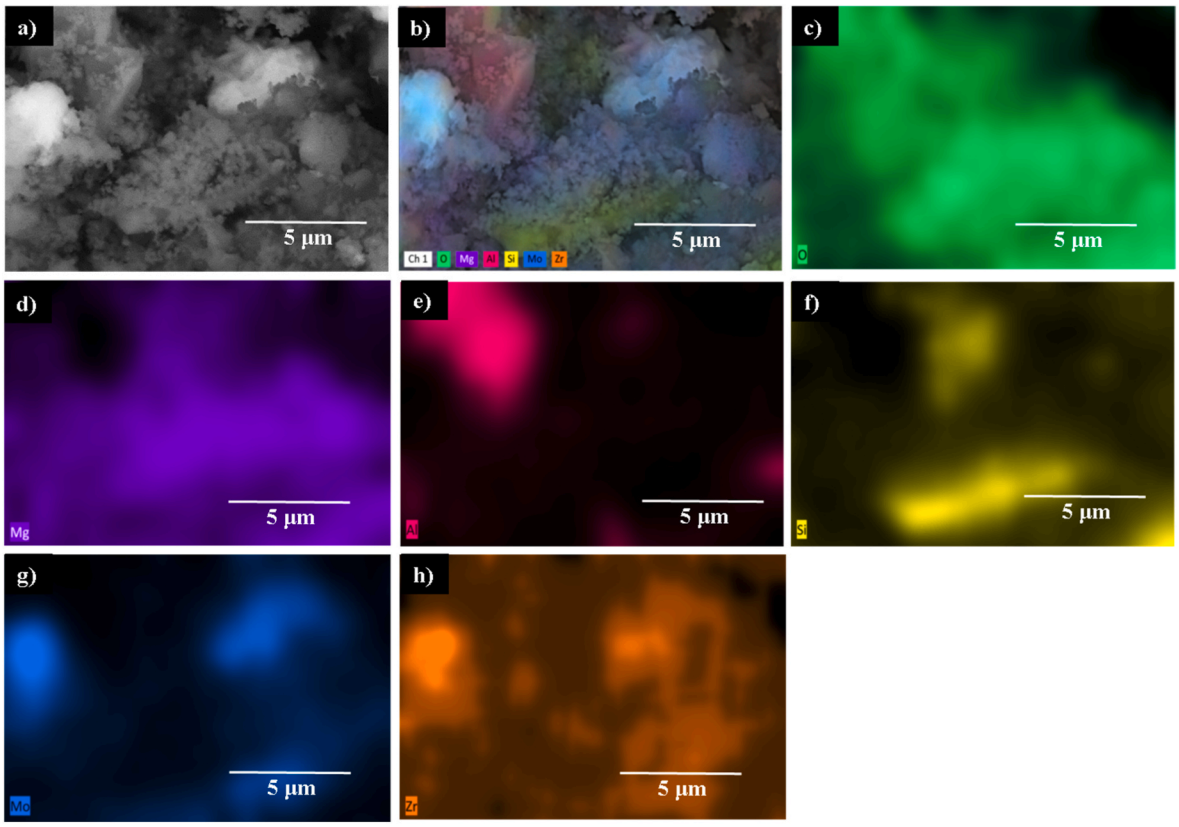

Fig. 19. Sample 2B sintered at 1200 °C for 2 h, a) backscattered electrons, b) Mapping of the constituent elements, c) Oxygen content, d) Magnesium, e) aluminum, f) Silicon, g) Molybdenum and h) zirconium.

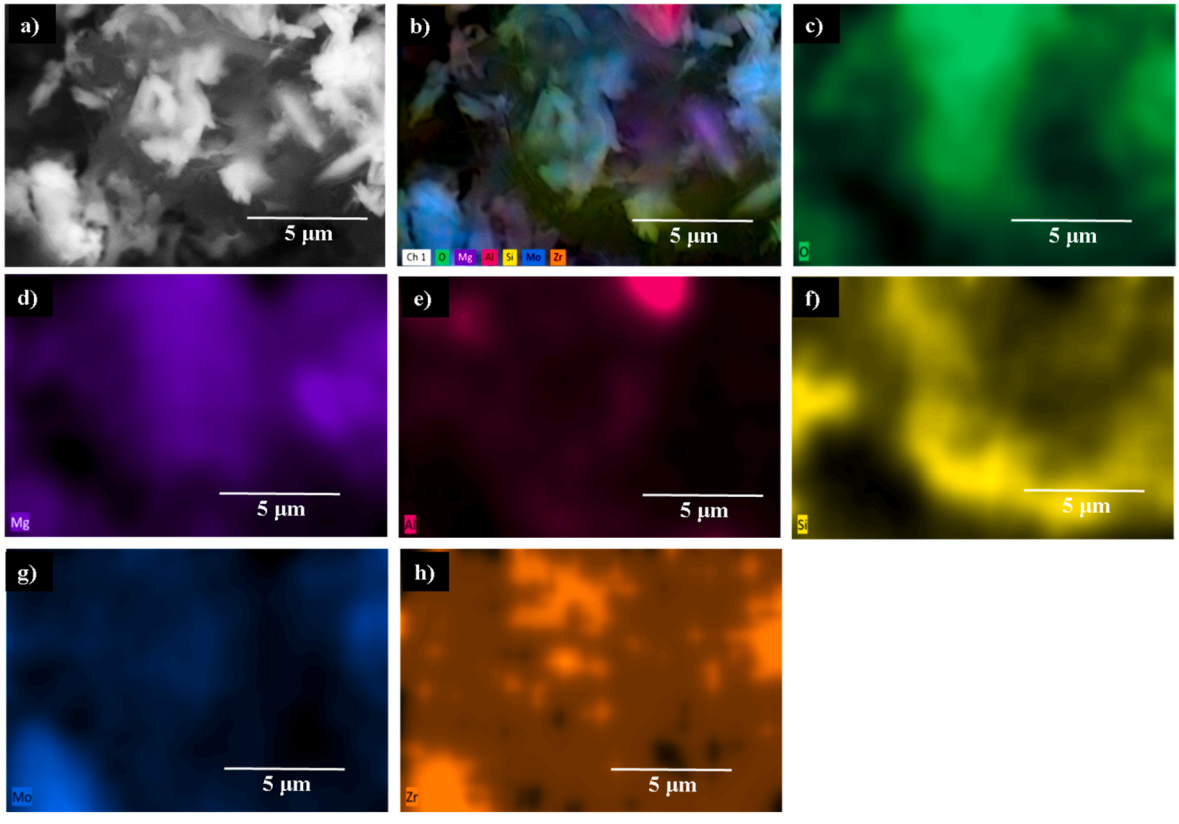

Fig. 20. Sample 2C sintered at 1200 °C for 2 h, a) backscattered electrons, b) Mapping of the constituent elements, c) Oxygen content, d) Magnesium, e) aluminum, f) Silicon, g) Molybdenum and h) zirconium.

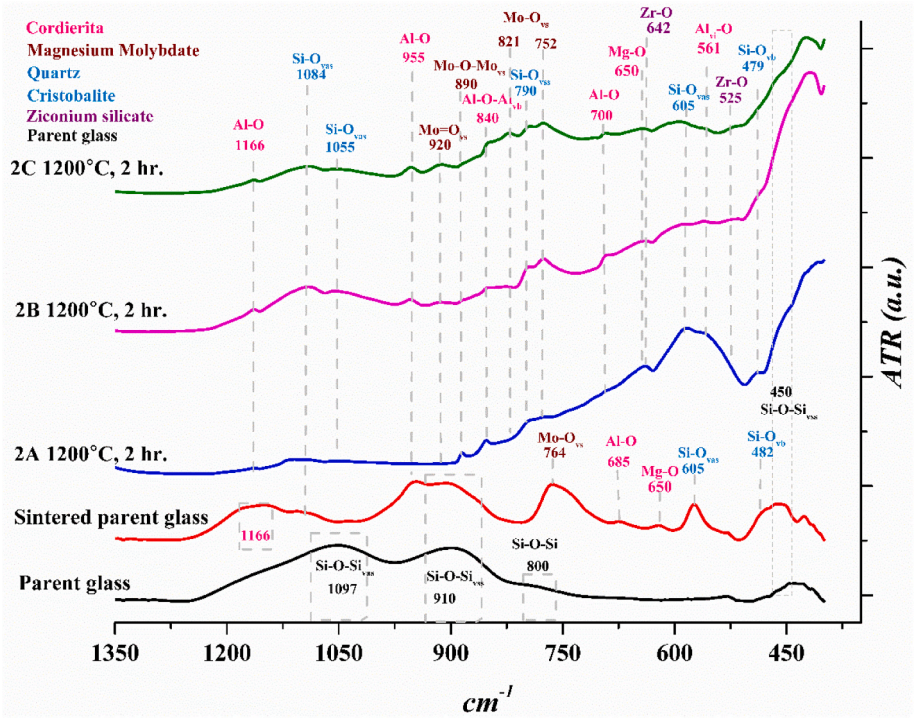

Fig. 21. Infrared spectra of samples after heat treatment at 1200 °C for samples parent glass, sintered parent glass, 2A, 2B y 2C.

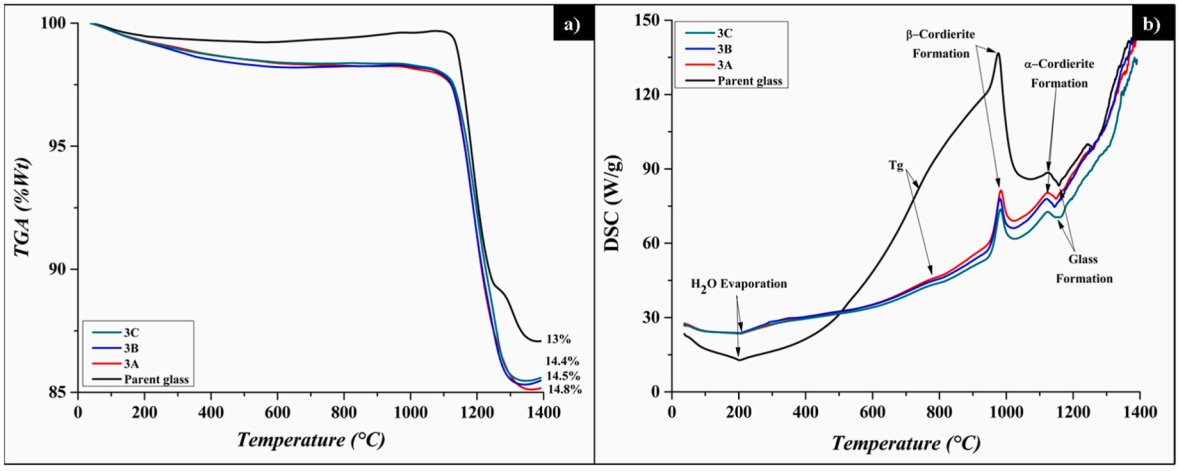

Fig. 22. a) TGA and b) DSC of Parent glass, samples 3A, 3B and 3C sintered at 1200 °C.

that corresponds to the crystallization of α cordierite and secondary phases such as SiO_2, silicates and aluminosilicates. Finally, an endothermic peak is observed in a range of 1150 °C that corresponds to the beginning of the glass melting, in this case the reactions of the samples that contain TiO_2, have temperatures very close to those of the reactions of the parent glass sample, for which can be said that TiO_2 does not promote cordierite crystallization to the same extent as NiO and ZrO_2.

Fig. 23 shows the diffractograms of the parent glass sample, parent glass sintered at 1200 °C, 3A, 3B and 3C, when using TiO_2 as nucleant, the crystalline phases identified are the following, α-cordierite, β-cordierite, mullite, magnesium molybdate, titanium-aluminum, quartz and cristobalite, when using TiO_2 as nucleating agent, the peaks of the phases obtained in samples 3A, 3B and 3C maintain the same intensity as those of the parent glass (see Fig. 18). With this it can be determined that TiO_2 does not help to increase the crystallization of the phases of interest, because TiO_2 behaves as a network breaker in the glass, which helps the formation of secondary phases such as mullite and titanium-aluminum oxide.

Fig. 24 shows the results of the phase quantification by the Rietveld method with the support of the High Score plus® software. In this case, a slight decrease in the sum of the percentage of cordierite phases is seen in comparison with the samples holding NiO and ZrO_2 (Figs. 8 and 16). As in the case of the samples that hold NiO and ZrO_2, the α-cordierite is the phase with the highest percentage in all the samples, followed by the β-cordierite; when adding values in the percentage range of 90.4 % to 84.4 %, they are obtained. As the percentage of TiO_2 increases, the sum of the total percentage of cordierite phases (α-cordierite + β-cordierite) decreases, since TiO_2 forms Mullite and Titanium Aluminum as a secondary phase in addition to the secondary phases that form in the case of samples holding NiO (Fig. 8). The formation of mullite and Titanium Aluminum causes the decrease in the formation of cordierite.

Fig. 25 shows the morphologies obtained by SEM analysis in samples 3A, 3B and 3C after heat treatment, Fig. 25a corresponds to sample 3A with a content of 1 % Wt. of TiO_2. In most cases, hexagonal flakes are

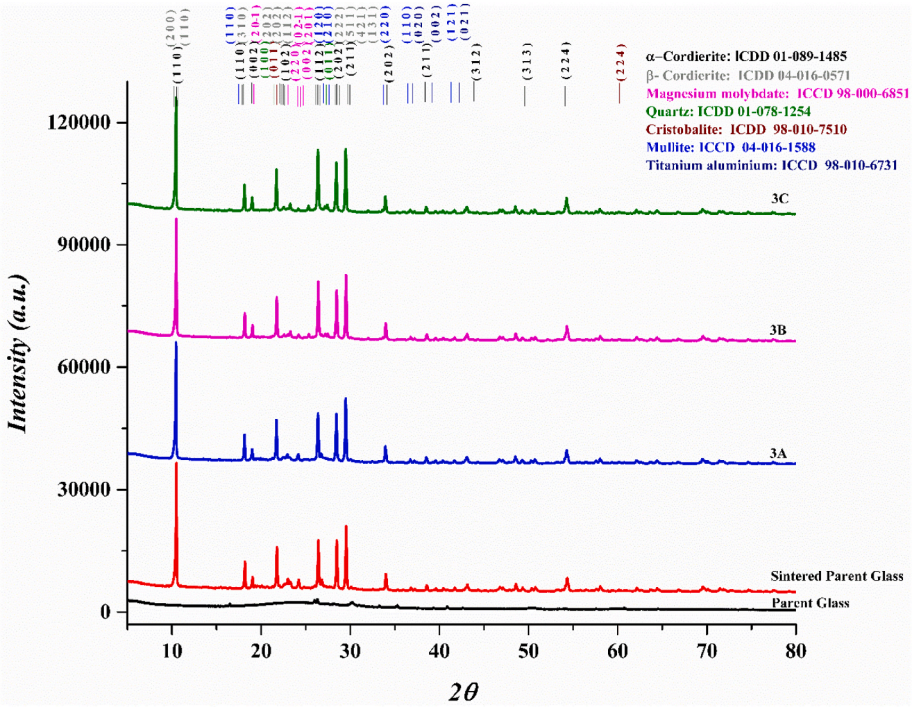

Fig. 23. X-ray diffraction of sample of parent glass, Sintered parent glass at 1200 °C, 3A, 3B y 3C.

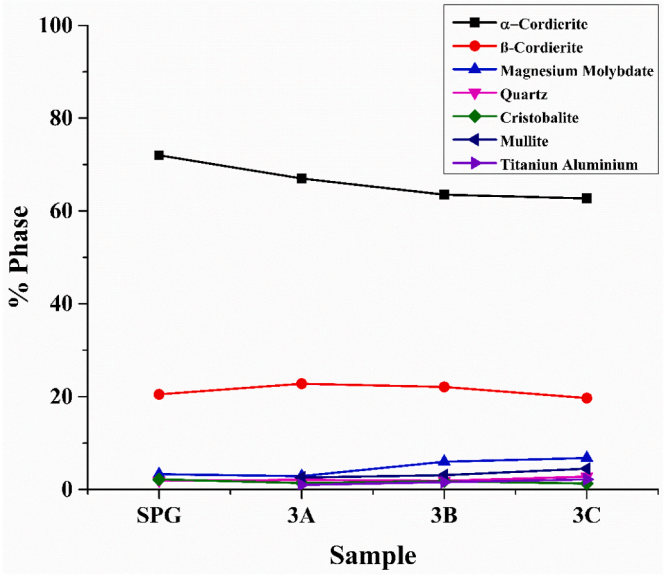

Fig. 24. X-Ray Diffraction Rietveld analysis at 1200 °C for samples parent glass, sintered parent glass, 3A, 3B y 3C.

observed, characteristic of the beginning of crystallization of the glass-ceramic α-cordierite; in Fig. 25b the morphology of the β-cordierite and some glassy phase particles are observed, in Fig. 25c the glassy phase and the morphology of β-cordierite are observed.

Figs. 26–28 show the results of the Elemental X-ray mapping for samples 3A, 3B and 3C respectively, where the presence of oxygen, magnesium, aluminum, silicon, molybdenum and titanium is observed; in the case of sample 3A (Fig. 26), a homogeneous distribution of oxygen, magnesium, aluminum, molybdenum and titanium is observed, which shows that there is homogeneity in the sample and the presence of the characteristic phases, the silicon is concentrated in a specific area which corresponds to glassy-phase particles. In sample 3B (Fig. 27), in the same way as in sample 3A, a homogeneous distribution of oxygen, magnesium, aluminum, molybdenum and titanium is observed, with a small concentration of silicon in a specific area that corresponds to the vitreous phase. In sample 3C (Fig. 28) a homogeneous distribution of oxygen, silicon, aluminum, molybdenum, and titanium is observed, which favors the formation of the phases of interest, in this case small concentrations of magnesium are observed, which may correspond to the formation of secondary phases such as mullite.

Fig. 29 shows the FT-IR spectra for the parent glass sample, parent glass sintered at 1200 °C, sample 3A, 3B and 3C. In this case, all the bands found in the samples holding NiO appear (Fig. 13). Additionally, it is possible to identify the bands at 690 cm^{-1} that correspond to the vibrations of the Ti–O bond [48–50]. There are also characteristic bands of mullite, at 823 cm^{-1} which is attributed to the stretching vibration of the Al–O bond and the band at 748 cm^{-1} which is attributed to the bending vibration of the Al–*O*–Al bond, although are at the Mo–O bonding positions, it can be seen that these two bands are more intense than in the FT-IR spectra of the samples containing NiO and ZrO_2, therefore the increase in intensity can be attributed to the characteristics of the bands of the mullite [32].

3. Final discussion

After reviewing the results obtained in this research project, it was seen through the phase quantification carried out by the Rietveld method with the support of the High Score Plus® software, that NiO works better as a nucleant, favoring the crystallization of the cordierite phases. As can be seen in the phase quantification results in Table 3, the highest percentage of cordierite phase is obtained in the samples that have NiO, which are in a range of 92.7%wt. and 95.7 % by weight. Also, as mentioned above, NiO does not form secondary phases with Parent Glass components, which can be supported by the X-ray diffraction phase identification results. However, the FT-IR results show the bands characteristics of the Ni–O bond, as well as in the mappings obtained by EDS (Figs. 10–12), the presence of Ni on the surface of the samples is identified, thus corroborating the presence of NiO in the structure, and based on the electronic properties (Table 1) of each of the elements that

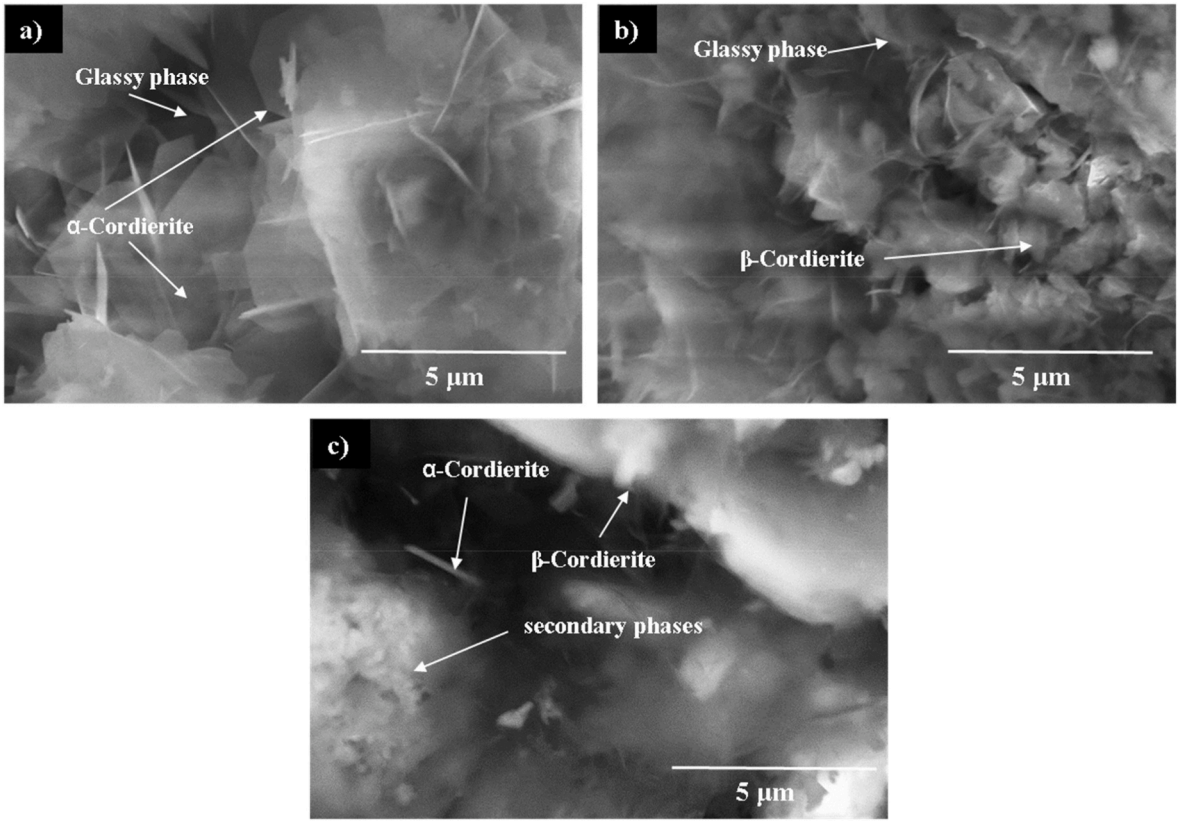

Fig. 25. Samples sintered at 1200 °C for 2 h, SEM secondary electrons, a) 3A, b) 3B and c) 3C.

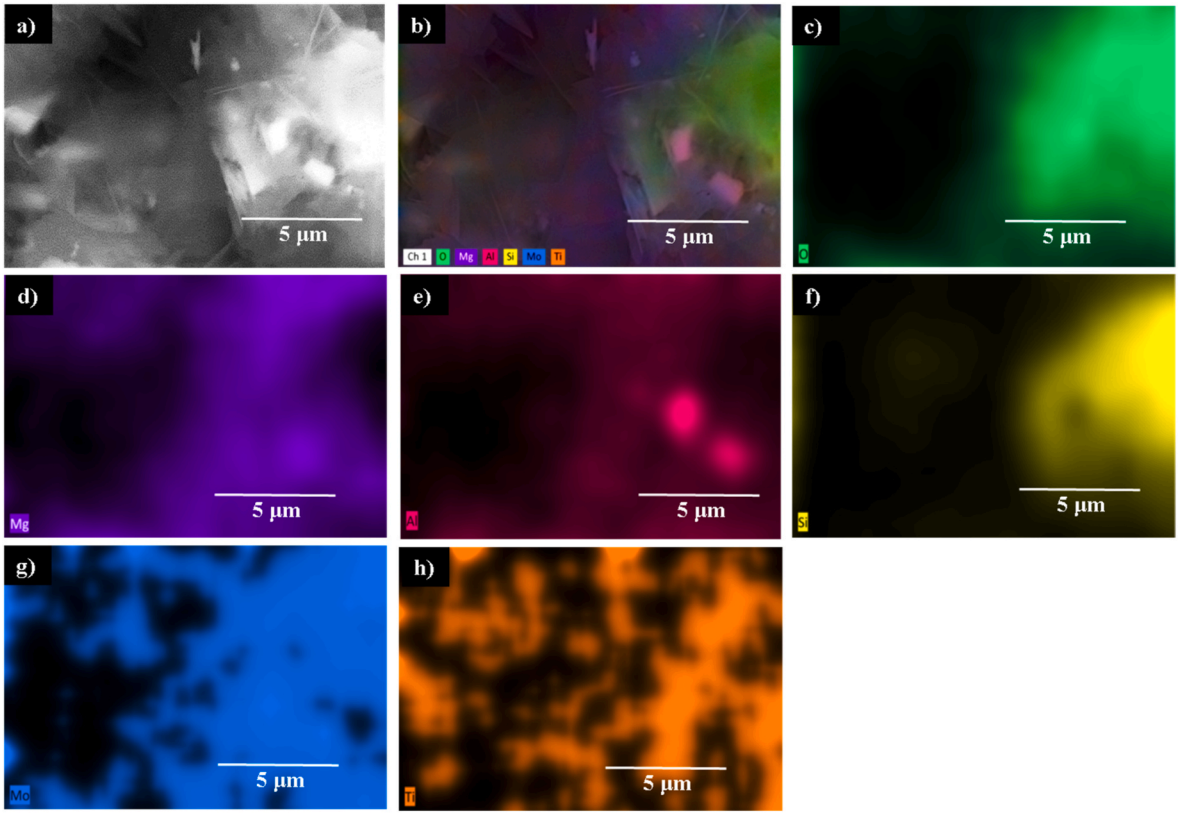

Fig. 26. Sample 3A sintered at 1200 °C for 2 h, a) backscattered electrons, b) Mapping of the constituent elements, c) Oxygen content, d) Magnesium, e) aluminum, f) Silicon, g) Molybdenum and h) titanium.

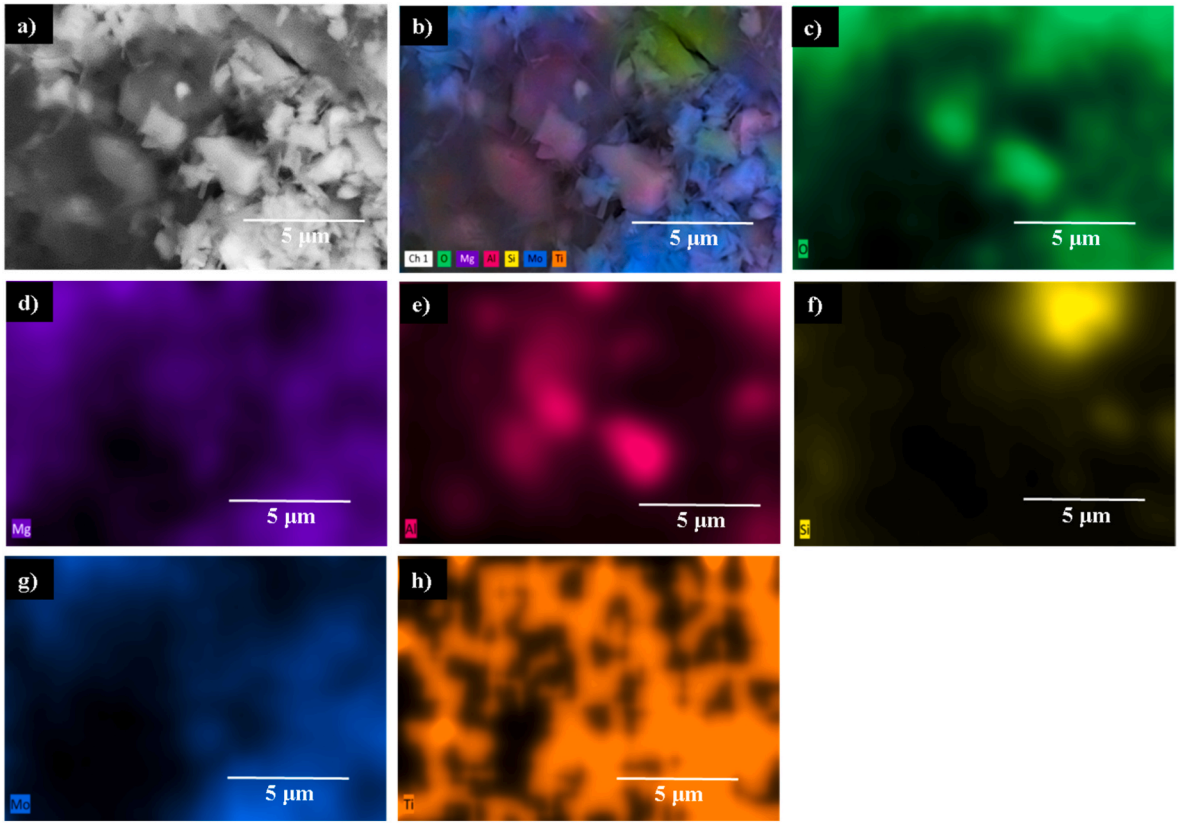

Fig. 27. Sample 3B sintered at 1200 °C for 2 h, a) backscattered electrons, b) Mapping of the constituent elements, c) Oxygen content, d) Magnesium, e) aluminum, f) Silicon, g) Molybdenum and h) titanium.

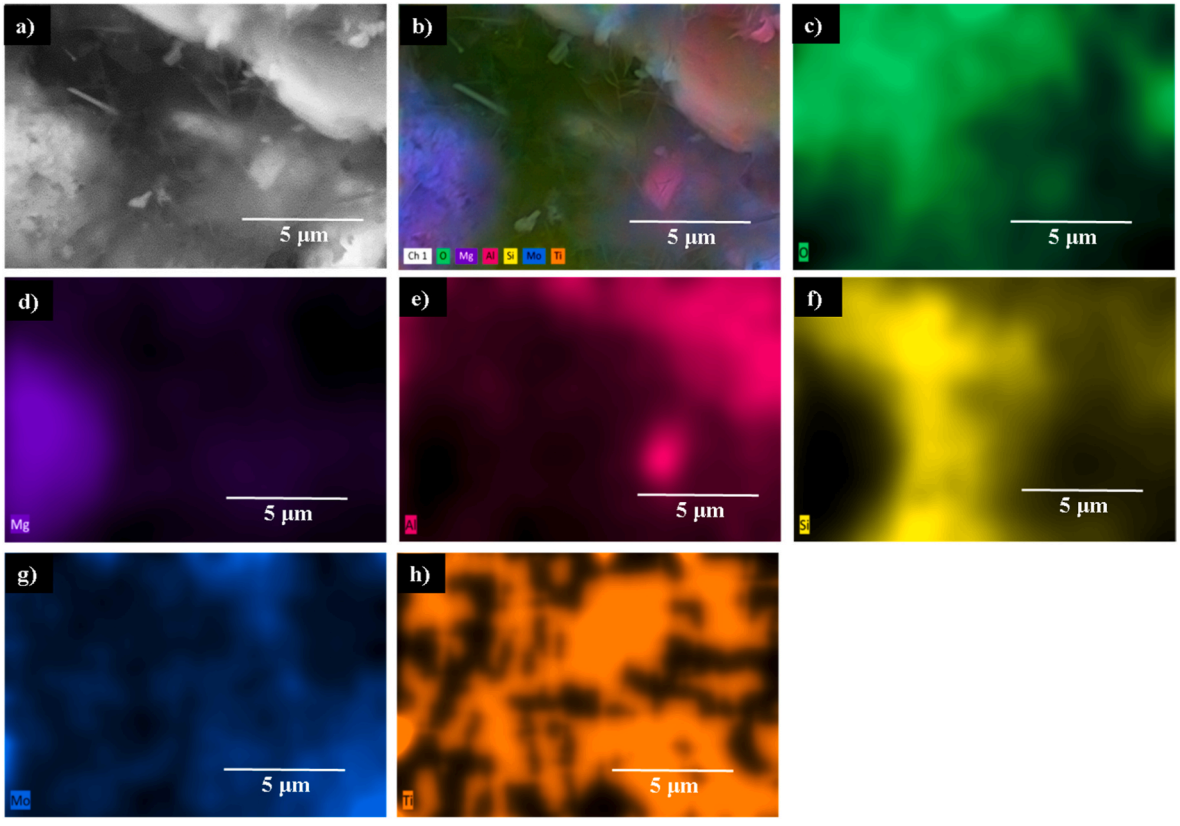

Fig. 28. Sample 3C sintered at 1200 °C for 2 h, a) backscattered electrons, b) Mapping of the constituent elements, c) Oxygen content, d) Magnesium, e) aluminum, f) Silicon, g) Molybdenum and h) titanium.

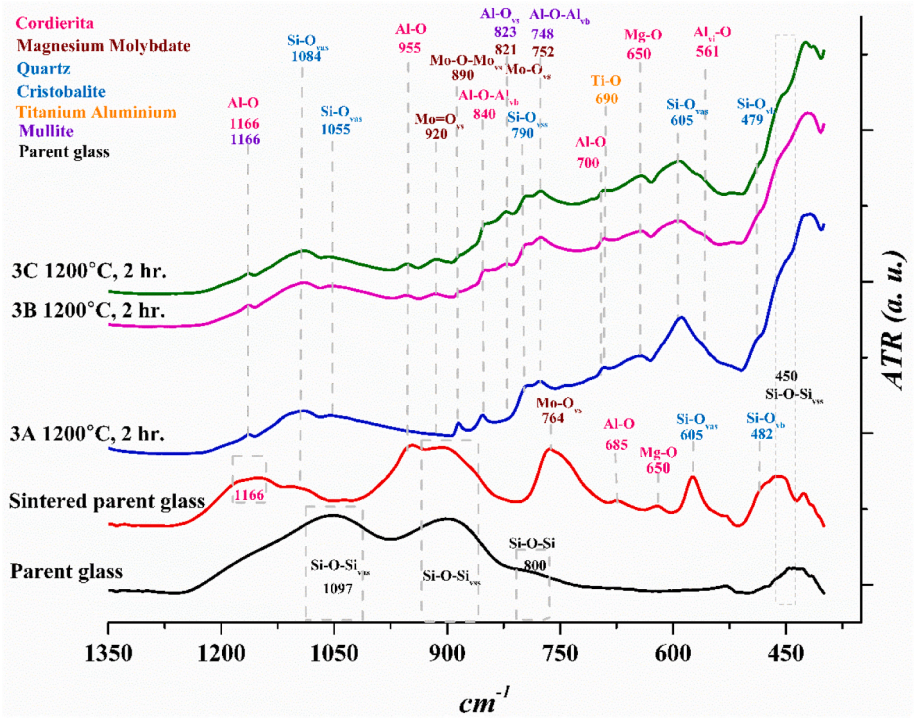

Fig. 29. Infrared spectra of samples after heat treatment at 1200 °C for samples parent glass, sintered parent glass, 3A, 3B y 3C.

Table 3
Phase quantification results.

Sample	α-Cordierite	β-Cordierite	Magensium Molybdate	Quartz	Cristobalite	Zirconium Silicate	Mullite	Titanium Aluminium	Cordierite Total	Secondary Phases Total
M7	72	20.5	3.3	1.9	2.2				92.5	7.5
M7-1A	66.6	29.1	2.4	1.5	0.4				95.7	4.3
M7-1B	65.9	28.1	3.9	1.8	0.3				94	6
M7-1C	64.9	27.8	4.6	2.4	0.3				92.7	7.3
M7-2A	59.1	35.3	0.3	0.8	0.3	4.3			94.1	5.7
M7-2B	56.5	39.2	0.7	0.7	0.5	2.3			95.7	4.3
M7-2C	63.7	22.7	4.6	2.3	2.1	4.6			86.4	13.6
M7-3A	67	23.8	2.9	2.1	1.4		2.6	0.1	90.8	9.2
M7-3B	63.5	23.6	6	1.9	1.8		3.1	0.1	87.1	12.9
M7-3C	62.7	21.7	6.8	2.8	1.3		4.5	0.2	84.4	15.6

are present in the samples, it is probable that Ni occupies the place of Al in the cordierite structure. In the case of ZrO_2 and TiO_2, by forming more secondary phases as determined by the identification and quantification of phases by X-ray diffraction, their efficiency in obtaining the phases of interest decreases, such as cordierite phases as observed in Table 3.

4. Conclusions

The uses of molybdenum as part of the MAS system help promote the formation of phases of interest, such as α and β cordierite, by reducing the crystallization temperature by at least 250 °C. However, NiO and ZrO_2 further promote cordierite formation by playing the role of nucleant in the crystallization of the α-cordierite and β-cordierite phases, even though ZrO_2 shows remarkably similar behavior to NiO when mixed. With cordierite original glass, ZrO_2 promotes the formation of secondary phases, which was shown by the identification and quantification of phases in the XRD results. On the other hand, when TiO_2 is used as a nucleant in the mixture, secondary phases such as mullite and aluminum-titanium oxide are formed. The XRD results show that the intensities of the reflections remain at the same intensity as those of the parent glass, which indicates that it does not promote the formation of the phases of interest, in addition to this, the quantification of phases reveals the decrease of the percentage of cordierite phases, so we finally conclude that NiO has the best effect on the mother glass, promoting the formation of α-cordierite and β-Cordierite. In addition, it does not form additional secondary phases, which guarantees obtaining a higher percentage of the phases of interest. Finally, with the results of the FT-IR and EDS mapping, the presence of Ni in the sample is demonstrated, as well as in the phases obtained, and since it has a percentage greater than 90 % of cordierite phases, it is likely that it is part of the structure.

Data availability

The data used to support the findings of this study are available from

the corresponding author upon request.

Conflict of interest

The authors declare that they have no conflict of interest.

Declaration of competing interest

The authors declare that they have no known competing financial interests or personal relationships that could have appeared to influence the work reported in this paper.

Acknowledgments

The authors gratefully acknowledge the financial support to Universidad Autónoma de Ciudad Juárez.

References

[1] Beall GH. Dr. S. Donald (Don) Stookey (1915–2014): pioneering researcher and adventurer, corning incorporated, corning, NY. USA Frontiers in Materials 2016. https://doi.org/10.3389/fmats.2016.00037.
[2] Deubenera J, Allixb M, Davisc MJ, Durand A, Höchee T, Honmaf T, Komatsuf T, Krügera S, Mitrag I, Müllerh R, Nakanei S, Pascuald MJ, Schmelzerj JwP, Zanottok ED, Zhoul S. Updated definition of glass-ceramics. J Non-Cryst Solids 2018;501(1):3–10. https://doi.org/10.1016/j.jnoncrysol.2018.01.033.
[3] Höland W, Beall G. Glass-ceramic technology. second ed. Hoboken: Wiley; 2012xvii–xx. 5-10.
[4] Stookey SD. (1958) history of the development of pyroceram, research management. In: Mc Millan PW, editor. Glass-eeramies. second ed. New York, London: Academic Press; 1979. https://doi.org/10.1080/00345334.1958.11755484. 1:3, 155.
[5] Vicente-Mingarro I, Callejas P, Rincon JM. Materiales vitrocerámicos: el proceso vitrocerámico. Bol. Soc. Esp. Ceram. Vidr. 1993;32(3):157–67. 1993, http://boletines.secv.es/upload/199332157.pdf.
[6] Vicente-Mingarro I. Estudio de los Mecanismos de Nucleación y Cristalización en vidrios obtenidos a partir de rocas basálticas canarias. Tesis Doctoral. Ed. U.C.M., 256, https://eprints.ucm.es/id/eprint/3093/1/T17770.pdf; 1992.
[7] Fernández N, El vidrio JM. Consejo superior de Investigaciones científicas, sociedad española de Cerámica y vidrio. Textos universitarios. ARTEGRAF, S.A. Tercera edición. Madrid España 2003;163. https://doi.org/10.1080/00345334.1958.11755484.
[8] Kingery WD. Introduction to ceramics. second ed. New York: John Wiley & Sons; 1976. p. 78–9. 448-514,532-40.
[9] Diaz AI. Síntesis y conformación de cordierita (2MgO.2Al2O3.5SiO2), para posibles aplicaciones como soporte catalítico. In: Facultad de Minas. vol. 60. Medellín: Universidad Nacional de Colombia; 2007.
[10] El-Shobaky HG, Fahmy YM. Cordierite as catalyst support for nanocrystalline CuO/Fe2O3 system. Mater Res Bull 2006;41(9):1701–13. https://doi.org/10.1016/j.materresbull.2006.02.015.
[11] Ali A, Abdelwahab SA, Abdelwahed K, Ahmed I, Ali AI. Influence of reinforcement oxides on structural and mechanical properties of glass-ceramics: a review article. Int J Innovative Technol Explor Eng 2021;10(5):117–27. https://doi.org/10.35940/ijitee.E8670.0310521.
[12] Moon K-T, Kim D-P. Preparation of porous cordierite with thermally stable pore structure. J Sol Gel Sci Technol 2003;26(1):229–34. https://doi.org/10.1023/A:1020751132432.
[13] Camerucci MA. Desarrollo y evaluación de Materiales cerámicos de Cordierita y cordierita-mullita. In: Facultad de Ingeniería. Mar del Plata: Universidad Nacional de Mar del Plata; 1999.
[14] Hipediger N. Liga Química Magnesia-Fosfato. Desarrollo y Aplicación en Cementos y Hormigones Refractarios. In: Área departamental construcciones. La Plata: Facultad de Ingeniería, Universidad Nacional de La Plata; 2007. p. 252. http://sedici.unlp.edu.ar/bitstream/handle/10915/1370/Documento_completo.pdf?sequence=31&isAllowed=y.
[15] Ali AI, Salim SA, Kamoun EA. Novel glass materials-based (PVA/PVP/Al2O3/SiO2) hybrid composite hydrogel membranes for industrial applications: synthesis, characterization, and physical properties. J Mater Sci Mater Electron 2022;33:10572–84. https://doi.org/10.1007/s10854-022-08043-w.
[16] Nahrawy, A. M. E., Hemdan, B. A., Ali, A. I., Youssef, A. M., and Abou H., A. B., "Sol-gel preparation of bioactive nanoporous (Al2O3: CuO: SiO2): dielectric properties and wastewater decontamination", Int J Mater Eng Innovat. 12, No. 1, https://doi.org/10.1504/IJMATEI.2021.113216..
[17] Radwan NRE, El-Shobaky GA, Fahmy YM. Cordierite as catalyst support for cobalt and manganese oxides in oxidation-reduction reactions. Appl Catal Gen 2004;274(1–2):87–99. https://doi.org/10.1016/j.apcata.2004.05.032.
[18] Barry TI, Cox JM, Morrell R. Cordierite glass-ceramics - effect of Tio 2 and Zro2 content on phase sequence during heat treatment. J Mater Sci 1978;13:594–610. https://doi.org/10.1007/BF00541810.
[19] Song K, Wu S, Liu P, Lin H, Ying Z, Zheng P, Su W, Deng J, Zheng L, Qin H. Phase composition and microwave dielectric properties of SrTiO3 modified Mg2Al4Si5O18 cordierite ceramics. J Alloys Compd 2015;628(57–62). https://doi.org/10.1016/j.jallcom.2014.12.199. ISSN 0925-8388.
[20] Hℓoland W, Rheinberger V, Schweiger M. Control of nucleation in glass ceramics. Phil Trans Roy Soc Lond 2003;361:575–89. https://doi.org/10.1098/rsta.2002.1152.
[21] Dargaud O, Cormier L, Menguy N, Galosy L, Calas G, Papin S, Querel G, Olivi L. Structural role of Zr4+ as a nucleating agent in a MgO-Al2O3-SiO2 glass-ceramics: a combined XAS and HRTEM approach. J Non-Cryst Solids 2010;356:2928–34. https://doi.org/10.1016/j.jnoncrysol.2010.05.104.
[22] Beall GH. Refractory glass-ceramics based on alkaline earth aluminosilicates. J Eur Ceram Soc 2009;29:1211–9. https://doi.org/10.1016/j.jeurceramsoc.2008.08.010.
[23] Golubkov VV, Chuvaeva TI, Dymshits OS, Shashkin AA, Zhilin AA, Byun W-B, Lee K-H. The influence of NiO on phase separation and crystallization of glasses of the MgO–Al2O3–SiO2–TiO2 system. J Non-Cryst Solids 2004;345/346:187–91. https://doi.org/10.1016/j.jnoncrysol.2004.08.020.
[24] Golubkov VV, Dymshits OS, Zhilin AA, Chuvaeva TI, Shashkin AV. The influence of nickel oxide additives on the phase separation and crystallization of glasses in the MgO–Al2O3–SiO2–TiO2 system. Glass Phys Chem 2004;30:300–10. https://doi.org/10.1023/B:GPAC.0000038701.82742.ec.
[25] Alekseeva I, Dymshits O, Golubkov V, Shashkin A, Tsenter M, Zhilin A, Byun WB. Phase transformations in NiO and CoO doped magnesium aluminosilicate glasses nucleated by ZrO2. Glass Technol 2005;46:187–91. http://www.ingentaconnect.com/content/sgt/gt/2005/00000046/00000002/art00033.
[26] Boberski C, Giess EA. Crystallization of nickel-bearing stoichiometric cordierite glasses. J Mater Sci 1994;29:67–72. https://doi.org/10.1007/BF00356574.
[27] Maeda K, Sera Y, Yasumori A. Effect of molybdenum and titanium oxides on mechanical and thermal properties of cordierite–enstatite glass-ceramics. J. Non-Cryst. Sol. 2016;434:13–22. https://doi.org/10.1016/j.jnoncrysol.2015.12.001.
[28] Abdelwahab SA, Ali A, Abdelwahed K, Ahmed I, Ali AI. Influence of TiO2/GO weight ratio on the structure, mechanical, and electrical properties of SiO2-Al2O3 glass-ceramics. J Mater Sci Mater Electron 2021;32:11092–106. https://doi.org/10.1007/s10854-021-05774-0.
[29] Maeda K, Yasumori A. Effect of molybdenum and tungsten oxides on nucleation and crystallization behaviors of MgO–Al2O3–SiO2 glasses. J. Non-Cryst. Sol. 2015;427:152–9. https://doi.org/10.1016/j.jnoncrysol.2015.07.040.
[30] Đorđević N, Obradović N, Kosanović D, Mitrić M, Pavlović VP. Sintering of cordierite in the presence of MoO3 and crystallization analysis. Sci Sinter 2014;46(3):307–13. https://doi.org/10.2298/SOS1403307D.
[31] Al-Otaibi AL. Yttrium doped single-crystalline orthorhombic molybdenum oxide micro-belts: synthesis, structural, optical and photocatalytic properties. J Inorg Organomet Polym 2021;31:3416–29. https://doi.org/10.1007/s10904-021-01999-y.
[32] Zalapa-Garibay MA, Torres-Torres D, Arizmendi-Morquecho AM, Reyes-López SY. Effect of NiO and MoO3 addition on the crystallinity and mechanical properties of α-cordierite and β-cordierite in the MgO-Al2O3-SiO2 system. Results Phys 2019;13:102227. https://doi.org/10.1016/j.rinp.2019.102227.
[33] Yu Y, Wang J, Yu Y, Yan Z, Du Y, Chu P, Jing Q, Liu P. Synthesis and characterization of single-phase α-cordierite glass-ceramics for LTCC substrates from tuff. Materials 2022;15:8758. https://doi.org/10.3390/ma15248758.
[34] Lu J, Wang H, Li Y, Zhou Y, Jiang W. Effect of metastable phase on the crystallization and mechanical properties of MgO-Al2O3-SiO2 glass-ceramics without nucleating agents. Ceram Int 2023;49(5):7737–45. https://doi.org/10.1016/j.ceramint.2022.10.278. ISSN 0272-8842.
[35] Xu X, Lao X. Effect of MgO/SiO2 ratio and Al2O3 content on crystallization behavior and properties of cordierite-based glass–ceramics. J Eur Ceram Soc 2021;41(2):1593–602. https://doi.org/10.1016/j.jeurceramsoc.2020.09.067. ISSN 0955-2219.
[36] Tang W, Zhang Q, Luo Z, Yu J, Gao X, Li Y, Lu A. CoO-doped MgO–Al2O3–SiO2-colored transparent glass–ceramics with high crystallinity. Appl Phys 2018;124:191. https://doi.org/10.1007/s00339-017-1537-6.
[37] Casasola R, Rincón J Ma, Romero M. Glass–ceramic glazes for ceramic tiles: a review. J Mater Sci 2011;47(2):553–82. https://doi.org/10.1007/s10853-011-5981-y.
[38] Baby JN, Sriram B, Wang S, George M, Govindasamy M, Benadict JX. Deep eutectic solvent-based manganese molybdate nanosheets for sensitive and simultaneous detection of human lethal compounds: comparing the electrochemical performances of M-molybdate (M = Mg, Fe, and Mn) electrocatalysts. Journal Nanoscale, The Royal Society of Chemistry 2020;12:19719–31. https://doi.org/10.1039/D0NR05533F.
[39] Nabil M, Mahmoud KR, El-Shaer A, Nayber HA. Preparation of crystalline silica (quartz, cristobalite, and tridymite) and amorphous silica powder (one step). J Phys Chem Solid 2018;121:22–6. https://doi.org/10.1016/j.jpcs.2018.05.001. ISSN 0022-3697.
[40] Lee T, Othman R, Yeoh F. Development of photoluminescent glass derived from rice husk. Biomass Bioenergy 2013;59:380–92. https://doi.org/10.1016/j.biombioe.2013.08.028. ISSN 0961-9534.
[41] Liu W, Zhao O, Zhao L, Shan Y. Short communication: collaborative adsorption and flotation of N-dodecyl ethylenediamine with short chain alcohol on quartz. Int J Electrochem Sci 2015;10(12):10188–98. https://doi.org/10.1016/S1452-3981(23)11252-1. ISSN 1452-3981.
[42] Zalapa-Garibay MA, Arizmendi-Morquecho A, Reyes-López SY. Low temperature synthesis of alpha alumina platelets and acicular mullite in MgO-Al2O3-SiO2 system 2019;10:9–18. https://doi.org/10.4416/JCST2018-00043.

[43] Kumar MS, Perumal AE, Vijayaram TR, Senguttuvan G. Processing and characterization of pure cordierite and zirconia-doped cordierite ceramic composite by precipitation technique. Bull Mater Sci 2015;38:679–88. https://doi.org/10.1007/s12034-015-0902-3.

[44] Eskandari M, Jahantigh F, Malekfar R. Synthesis and characterization of nanosized pure α-cordierite glass-ceramic powders. J Australas Ceram Soc 2018;54:243–9. https://doi.org/10.1007/s41779-017-0147-2.

[45] Torres FJ, Rodríguez-Mendoza UR, Lavín V, Ruiz de Sola E, Alarcón J. Evolution of the structural and optical properties from cobalt cordierite glass to glass-ceramic based on spinel crystalline phase materials. J Non-Cryst Solids 2007;353(44–46):4093–101. https://doi.org/10.1016/j.jnoncrysol.2007.06.014. ISSN 0022-3093.

[46] Moavi J, Buazar F, Sayahi MH. Algal magnetic nickel oxide nanocatalyst in accelerated synthesis of pyridopyrimidine derivatives. Sci Rep 2021;11:6296. https://doi.org/10.1038/s41598-021-85832-z.

[47] Shanaghi A, Souri AR, Rafie M, Chu PK. Effects of Benzotriazole on nano-mechanical properties of zirconia–alumina–Benzotriazole nanocomposite coating deposited on Al 2024 by the sol–gel method. Appl Phys 2019;125:728. https://doi.org/10.1007/s00339-019-3022-x.

[48] Al-Amin M, Chandra Dey S, Ur Rashid T, Ashaduzzaman Md, Shamsuddin S. Solar assisted photocatalytic degradation of reactive azo dyes in presence of anatase titanium dioxide, vol. 2; 2016. p. 14–21. http://www.ijlret.com/Papers/Vol-2-issue-3/14-B2016126.pdf. 3.

[49] Wang Hao, Wang Shaoxin, Zhao Meng, Chen Ziwei, Liu Lili, Wang Xidong, Qian Dayi, Xing Yi. Mechanism of cordierite formation obtained by high temperature sintering technique. Ceram Int 2023;49(12):20544–55. https://doi.org/10.1016/j.ceramint.2023.03.184. ISSN 0272-8842.

[50] Majerová M, Prnová A, Plško, Hruška B, Valúchová J, Kraxner J, Bruneel E, Buysser KD, Galusek D. Crystallization kinetics of Ni-doped Ca2Al2SiO7 glass microspheres. J Therm Anal Calorim 2020;142:2111–21. https://doi.org/10.1007/s10973-020-10154-7.